Studies on development of novel therapeutic agent against RNA virus infection

（RNA ウイルス感染症に対する新規治療薬の開発に関する研究）

Haruaki Nobori

Contents

Abbreviations

3CL:	3C-like
A119S:	Alanine-to-serine at amino acid position 119
Ae. aegypti:	*Aedes aegypti*
Ae. albopictus:	*Aedes albopictus*
AAALAC:	Association for Assessment and Accreditation of Laboratory Animal Care
ACTB:	Actin Beta
ANOVA:	Analysis of variance
C87S:	Cystatin-to-serine at amino acid position 87
CC_{50}:	50% cytotoxicity concentration
cDNA:	Complementary DNA
COVID-19:	Coronavirus disease 2019
CPE:	Cytopathic effect
DENV1-4:	Dengue virus type 1-4
DMEM:	Dulbecco's modified Eagle's medium
DMSO:	Dimethyl sulfoxide
DPBS:	Dulbecco's PBS
dpi:	day post-infection
DTT:	dithiothreitol
EC_{50}:	50% effective concentration
EC_{90}:	90% effective concentration
ELISA:	Enzyme-linked immunosorbent assay
EMEM:	Eagle's minimum essential medium
ER:	Endoplasmic reticulum
FBS:	Fetal bovine serum
fLuc:	firefly luciferase
FR:	Fold resistance
G124A:	Glycine-to-alanine at amino acid position 124
GAPDH:	glyceraldehyde-3-phosphate dehydrogenase
GTase:	Guanylyl transferase
GTP:	Guanosine triphosphate
H&E:	Hematoxylin and Eosin
h:	hour
HCV:	Hepatitis C virus

HIV:	Human immunodeficiency virus
HMGCR:	3-hydroxy-3-methylglutaryl-Coenzyme A reductase
hpi:	hours post-infection
hpt:	hours post transfection
IFN:	Interferon
IHC:	Immunohistochemical
IL:	Interleukin
IPTG:	Isopropyl-β-D-thiogalactopyranoside
IRF3:	Interferon regulatory factor 3
JEV:	Japanese encephalitis virus
kb:	kilobase
L206P:	Leucine-to-proline at amino acid position 206
LLOQ:	Lower limit of quantification
M196V:	Methionine-to-valine at amino acid position 196
M37I:	Methionine-to-isoleucine at amino acid position 37
M85T:	Methionine-to-threonine at amino acid position 85
MAVS:	Mitochondrial antiviral signaling
MC:	Methylcellulose 400 cP
MCP-1	Monocyte chemoattractant protein-1
MEM:	Minimal Essential Medium
min:	minute
MOI:	Multiplicity of infection
MTase:	Methyltransferase
MTT:	3-[4,5-dimethyl-2-thiazolyl]-2,5-diphenyl-2H-tetrazolium bromide
N246D:	Asparagine-to-aspartic acid at amino acid position 246
NC:	Negative control
NIID:	National Institute of Infectious Diseases
NLRP12:	NLR family pyrin domain containing 12
NS:	Non-structural protein
nt:	nucleotide
NT:	Not tested
PBS:	Phosphate-buffered saline
PC:	Positive control
PCR:	Polymerase chain reaction
pTMDs:	predicted transmembrane domains
RdRp:	RNA-dependent RNA polymerase

RIG-I: Retinoic acid-inducible gene-I
RLU: Relative Light Unit
RPMI: Roswell Park Memorial Institute
RT-qPCR: quantitative reverse transcription PCR
S186F: Serine-to-phenylalanine at amino acid position 186
SAH: S-Adenosyl-L-homocysteine
SAM: S-Adenosyl-L-methionine
SARS-CoV-2: Severe acute respiratory syndrome coronavirus 2
SD: Standard deviation
T120K: Threonine-to-lysine at amino acid position 120
T244I: Threonine-to-isoleucine at amino acid position 244
$TCID_{50}$: 50% tissue culture infectious dose
TGF-β: Transforming growth factor-β
TLC: Thin-layer chromatography
TMPRSS-2: Transmembrane serine protease 2
TNF-α: Tumor necrosis factor-α
Tris-HCl: Tris(hydroxymethyl)aminomethane hydrochloride
UTR: Untranslated region
V130A: Valine-to-alanine at amino acid position 130
VeroE6/TMPRSS2: TMPRSS2-expressing VeroE6
WHO: World Health Organization
WNV: West Nile virus
WT: Wild-type
Y97C: Tyrosine-to-cysteine at amino acid position 97
YFV: Yellow Fever virus
ZIKV: Zika virus

Notes

Contents of the present thesis were published in the following articles.

Chapter I

Nobori H, Toba S, Yoshida R, Hall WW, Orba Y, Sawa H, Sato A. Identification of Compound-B, a novel anti-dengue virus agent targeting the non-structural protein 4A. *Antiviral Res*, 155, 60-66, 2018.

Nobori H, Uemura K, Toba S, Sanaki T, Shishido T, Hall WW, Orba Y, Sawa H, Sato A. Identification of quinolone derivatives as effective anti-Dengue virus agents. *Antiviral Res*, 184, 104969, 2020.

Chapter II

Nobori H, Fukao K, Kuroda T, Anan N, Tashima R, Nakashima M, Noda S, Tajiri M, Torii M, Toba S, Uemura K, Sanaki T, Shishido T, Tachibana Y, Kato T. Efficacy of ensitrelvir against SARS-CoV-2 in a delayed-treatment mouse model. *J Antimicrob Chemother*, 77 (11), 2984-2991, 2022.

General Introduction

Various RNA virus, including dengue virus (DENV)[1, 2] and severe acute respiratory syndrome coronavirus 2 (SARS-CoV-2)[3] infections have occurred and become prevalent all over the world[4, 5]. Vaccines have been developed to suppress infection and aggravation, but therapeutic drugs are also required to control infectious diseases.

DENV causes a widespread endemic disease known as dengue fever and dengue hemorrhagic fever, which is one of the most serious infectious diseases in tropical and subtropical areas[6-8]. Approximately 390 million DENV infections, resulting in 96 million cases of clinical disease, occur each year worldwide[1, 2]. DENV is transmitted by mosquitoes primarily *Aedes aegypti* (*Ae. aegypti*) and *Aedes albopictus* (*Ae. albopictus*)[9]. Moreover, the increasing habitat range of the DENV mosquito vectors, *Ae. aegypti* and *Ae. albopictus*, has resulted in an increase in the global spread of DENV[9, 10]. Some DENV vaccines have been licensed[11-15]; however, it is not yet possible to fully control DENV infections. Also, despite global efforts, no antiviral drug is available for the clinical treatment of DENV infection[16] and there is a demand for the development of antiviral drugs.

SARS-CoV-2, the etiological agent of coronavirus disease 2019 (COVID-19), was first identified in Wuhan, Hubei Province, People's Republic of China in December 2019. The World Health Organization (WHO) declared the SARS-CoV-2 outbreak a Public Health Emergency of International Concern on 30 January 2020 and subsequently a pandemic on 11 March 2020. COVID-19 remains a global health crisis with over 649 million confirmed cases and over 6.6 million reported deaths worldwide as of 21 December 2022[3]. Vaccination against SARS-CoV-2 has been promoted throughout the world. However, some of virus encoding proteins affect on virus infectivity and pathogenicity and allow the virus to evade host immune surveillance. Thus, SARS-CoV-2 may continue to be a problematic health issue. Although there are some approved oral therapeutic drugs (molnupiravir and nirmatrelvir/ritonavir), there are concerns about insufficient efficacy, safety, drug interactions, etc., and the development of new therapeutic drugs is highly desirable.

Antiviral drugs are developed through many processes. At the early stage of drug discovery, *in vitro* compound screening was performed using enzyme assay which specifically possessed in virus or virus replication inhibitory assay with virus-infected cells to acquire seeds of antiviral drug candidate. The antiviral activity of initial seed compounds are usually insufficient, therefore it is necessary to modify the structure of

seed compounds to improve their antiviral activity. Furthermore, it is important to maintain a constant plasma or viral target organ concentration of compound *in vivo* to show antiviral activity, therefore, it is also required to optimize the structure in consideration of pharmacokinetics such as metabolic stability, oral absorption, and distribution. Antiviral drug candidates with improved antiviral activity and pharmacokinetics proceed to the next stage of drug discovery. At the late stage of drug discovery, compounds which show not only *in vitro* efficacy such as viral enzyme inhibitory activity or antiviral activity in cells, but also *in vivo* efficacy in infection models using animals such as mice and hamsters in pharmacological evaluation, are selected as antiviral drug candidates that may show therapeutic efficacy in the clinical phase.

In this study, to develop novel antiviral drugs against DENV and SARS-CoV2, appropriate assays for evaluation of antiviral activity were established. In Chapter I, assays for anti-DENV compound screening at the early stage of drug discovery were established and the seeds of antiviral drug candidate against DENV infection were identified. In Chapter II, at the late stage of drug discovery, *in vivo* efficacy of ensitrelvir (S-217622), COVID-19 therapeutic drug candidate, was evaluated using a SARS-CoV-2 infection mouse model.

Chapter I: Identification of Compound-B, Compound-X, and Compound-Y as novel anti-dengue virus agents

Introduction

DENV is a positive-sense single-stranded RNA virus belonging to the *Flaviviridae* family and the genus *Flavivirus* and has four known serotypes. The genus *Flavivirus* also includes West Nile virus (WNV), Japanese encephalitis virus (JEV), yellow fever virus (YFV), and Zika virus (ZIKV), which all cause disease in humans[17]. DENV contains an 11-kilobaese (kb) positive-sense, single-stranded RNA genome consisting of a single open reading frame encoding three structural proteins (C, prM, and E), which form the viral particle, and seven non-structural proteins (NS1, NS2A, NS2B, NS3, NS4A, NS4B, and NS5), which participate in viral RNA genome replication[6, 18-20]. Among these non-structural proteins, NS5 contains the N-terminal guanylyl transferase (GTase) and methyltransferase (MTase) domains[21, 22] and the C-terminal RNA-dependent RNA polymerase (RdRp) domain[23, 24].

In this study, a cell-based assay using DENV type 2 (DENV2) infected BHK-21 cells was established and antiviral activity of about 7,000 compounds retrieved from Shionogi & Co., Ltd. antiviral compounds library, including compounds with activities against hepatitis C virus (HCV) and human immunodeficiency virus (HIV), were investigated to find a novel seeds of antiviral drug candidate at the early stage of drug discovery.

As a result, three novel compounds (Compound-B, Compound-X, and Compound-Y) with anti-DENV activity were identified. Further investigation has been performed about these compounds by generating compound-resistant DENV2 and analyzed the amino acid substitutions found in these compound-resistant viruses.

Materials and methods

Cells and viruses

Baby hamster kidney cell line BHK-21 cells and human lung adenocarcinoma epithelial cell line A549 cells were maintained in high-glucose Dulbecco's modified Eagle medium (DMEM) supplemented with 10% fetal bovine serum (FBS) at 37°C, 5% CO_2. C6/36 cells were maintained in Eagle's minimum essential medium (EMEM) supplemented with 10% FBS, nonessential amino acids, and sodium pyruvate at 28 °C, 5% CO_2. The following DENV serotypes were used in this study: DENV1 (D1/hu/PHL/10-07), DENV2 (D2/hu/INDIA/09-74, accession number LC367234), DENV3 (D3/hu/Thailand/00-40), and DENV4 (D4/hu/Solomon/09-11). Other flaviviruses, i.e., WNV (NY99 strain), YFV (17D-204 strain), ZIKV (MR766 strain), and JEV (Beijing-1 strain) were used for counter screening.

Reagents

Ribavirin, mycophenolic acid, and sinefungin were purchased from Sigma-Aldrich Corporation (St. Louis, MO, USA). All compounds used for screening were synthesized by Shionogi & Co., Ltd. (Osaka, Japan). These compounds were dissolved in dimethyl sulfoxide (DMSO) and maintained as stock solutions.

Cell viability assays

The MTT (3-[4,5-dimethyl-2-thiazolyl]-2,5-diphenyl-2H-tetrazolium bromide) assay was performed to calculate cell viability following viral infection according to methods previously described[25]. In the case of DENV, BHK-21 cells (3.0×10^4 cells/well) suspended in EMEM supplemented with 2% FBS were seeded into 96-well plates with diluted compounds in each well. After incubation for 1 hour (h) at 37°C, DENV2 was added at a multiplicity of infection (MOI) of 0.01. Following incubation for 4 days, the 5 mg/mL MTT reagent (Sigma-Aldrich Corporation) was added to each well and the plate was incubated at 37 °C for 2 h. After incubation, the culture supernatants were removed and cell lysis solution (2-propanol with 10% Triton-X 100, and 0.31% HCl) was added. Absorbance at a wavelength of 560 nm and reference wavelength of 690 nm was measured using a microplate reader (model 680; Bio-Rad Laboratories, Hercules, CA, USA), and then the 50% effective concentration (EC_{50}) was calculated using the two-point method. Cell toxicity was assessed with the same condition as in the measurement of anti-DENV activity, and the 50% cytotoxicity concentration (CC_{50}) was calculated using the two-point method. In the case of other flaviviruses, BHK-21 cells were cultured

in Roswell Park Memorial Institute (RPMI) 1640 medium supplemented with 10% FBS and then seeded at a concentration of 2.0×10^4 cells/well of YFV or 2.5×10^5 cells/well for WNV, JEV, and ZIKV. Each virus was infected 4–10 of 50% tissue culture infectious dose ($TCID_{50}$)/well and the assay endpoint was 3 days.

Selection of compound-resistant DENV2

DENV2-infected and non-infected BHK-21 cells were seeded into the same wells in the presence of compound. When a cytopathic effect (CPE) was observed, DENV2-infected culture supernatants were transferred to non-infected BHK-21 cells in the presence of the compound. Passages were performed every 2–3 days. The concentration of Compound-B was 3.4 μM for the first 6 days and was increased to 6.8 μM for an additional 14 days incubation. The concentration of Compound-X was 11.8 μM for 10 days followed by 23.5 μM for 20 days, and the concentration of Compound-Y was 11.0 μM for 10 days followed by 22.0 μM for 20 days. The passaged viruses were collected and cloned by the plaque method (described below). The supernatants from DENV2-infected cells after 20 or 30 days in the absence of compounds were used as controls (passaged-DENV2).

Genome sequence analysis

Full genome sequence analysis was performed using an Ion PGM system (Life Technologies, Carlsbad, CA, USA), as previously described[26]. Briefly, viral RNA was extracted using the Pure-Link Viral RNA/DNA mini kit (Thermo Fisher Scientific, San Jose, CA, USA) and the double-stranded complementary DNA (cDNA) was synthesized with a sequence-tagged random hexamer (5′-CGC TCT TCC GAT CTN NNN NN-3′)[27] using the PrimeScript Double Strand cDNA Synthesis Kit (Takara Bio, Inc., Shiga, Japan). Double-stranded cDNA was amplified with KOD-plus-Neo DNA polymerase (Toyobo, Co. Ltd., Tokyo, Japan) and a tag sequence primer (5′-CGC TCT TCC GAT CT-3′). The polymerase chain reaction (PCR) products were fragmented using a Covaris S2 focused-ultrasonicator (Covaris, Woburn, MA, USA) and used to prepare a 400-baseread library using the Ion Plus Fragment Library kit (Life Technologies, Gaithersburg, MD, USA) and E-Gel SizeSelect 2% agarose gels (Life Technologies). Emulsion PCR was performed using the Ion PGM Template Hi-Q OT2 400 kit (Life Technologies). Sequencing was performed using an Ion PGM sequencer with an Ion PGM Sequencing 400 kit and the Ion 318 Chip V2 (Life Technologies). Data analysis was performed with CLC Genomics Workbench ver. 7.5.1 software (CLC bio Japan, Tokyo, Japan).

Construction of recombinant and mutant DENV2 infectious clones

Recombinant DENV2 (D2/hu/INDIA/09-74) was synthesized by modifying rDENV-1(02-20)/pMW119[28]. DENV2 genomic RNA was extracted from the culture supernatant of the DENV2-infected C6/36 cells using the PureLink viral RNA/DNA mini kit (Thermo Fisher Scientific), and viral cDNA was obtained using SuperScript III Reverse Transcriptase (Thermo Fisher Scientific) with random hexamers. The RNA viral genome was amplified with KOD-plus-Neo DNA polymerase (Toyobo, Co. Ltd.) with the primers listed in Table 1. Each cDNA was inserted into a pMW119 vector using an In-Fusion HD cloning kit (TaKaRa Bio, Inc.), according to the manufacturer's protocol. Four intermediate clones containing i) the T3 promoter with the DENV2 genome of 1–2,208 nucleotides (nt) (DENV2-1/pMW119), ii) 2,195–5,431 nt (DENV2-2/pMW119), iii) 5,426–8,754 nt (DENV2-3/pMW119), or iv) 7,420–10,723 nt (DENV2-4/pMW119) were constructed. Next, a plasmid containing the whole DENV2 genome (DENV2/pMW119) was constructed using the four intermediate plasmids described above and the cloning reaction was performed. A point mutation for prM, NS4A, and NS4B were inserted in the intermediate clones by amplifying with the primers listed in Table 2 and replaced with DENV2/pMW119. A point mutation fragment for E, NS1, and NS5 was amplified with the primers listed in Table 2 and inserted into DENV2/pMW119.

***In vitro* transcription, transfection, and preparation of viral solutions**

The T3 promoter and DENV2 genomic region in DENV2/pMW119 were amplified using the two primers, T3p_Fw (5'-CTG CAA GGC GAT TAA GTT GGG TAA C-3') and D2_10723nt_Rv (5'-AGA ACC TGT TGA TTC AAC AGC A-3'). DENV2 genomic RNA was generated as previously described[28]. Briefly, the synthesized DENV2 genomic RNA was used to transfect BHK-21 cells with Lipofectamine MessengerMAX reagent (Thermo Fisher Scientific). The cell culture supernatants were collected when a CPE was observed.

Table 1. Primer list for construction of DENV2 infectious clones

Primer name	Sequence 5'->3'	Template	Constructed plasmid
D2_1nt_Fw	AGTTGTTAGTCTACGTGGACCGA	DENV2 cDNA	DENV2-1/pMW119
pMW_D2_2208nt_Rv	CCAAGCTTGGATCCAAAATCCC		
D2_2202nt_pMW_Fw	TGGATCCAAGCTTGGCGTAATCA	rDENV-1(02-20)/pMW119	
D2_15nt_T3_pMW_Rv	CGTAGACTAACAACTCCCTTTAGTGAGGGTTAATTCC		
pMW_D2_2195nt_Fw	GTACCCGGGATTTTGGATCCCTG	DENV2 cDNA	DENV2-2/pMW119
pMW_D2_5431nt_Rv	CCAAGCTTCTCGAGTTGAAATGTATCCT		
D2_5425_pMW_Fw	ACTCGAGAAGCTTGGCGTAATCATG	rDENV-1(02-20)/pMW119	
D2_2203_pMW_Rv	CAAAATCCCGGGTACCGAGCTCGAA		
pMW_D2_5426nt_Fw	ATTCGAGCTCGAGTAGAGATGGG	DENV2 cDNA	DENV2-3/pMW119
pMW_D2_8758nt_Rv	CCAAGCTTCTCTAGTGCACATCC		
D2_8752_pMW_Fw	ACTAGAGAAGCTTGGCGTAATCATGG	rDENV-1(02-20)/pMW119	
D2_5433_pMW_Rv	TACTCGAGCTCGAATTCACTGGC		
pMW_D2_7420nt_Fw	GTACCCGGGCCCATTTCCACATTG	DENV2 cDNA	DENV2-4/pMW119
D2_10723nt_Rv	AGAACCTGTTGATTCAACAGCA		
D2_10709_pMW_Fw	GAATCAACAGGTTCTCCGCGGAAGCTTGGCGTAATCATGGTC	rDENV-1(02-20)/pMW119	
D2_7428_pMW_Rv	AATGGGCCCGGGTACCGAGCTCGAATTCA		
D2_10709_pMW_Fw	GAATCAACAGGTTCTCCGCGGAAGCTTGGCGTAATCATGGTC	DENV2-1/pMW119	DENV2/pMW119
D2_2218nt_Rv	CTCCTCCCAGGGATCCAAAATCCCAG		
D2_2204nt_Fw	GATCCCTGGGAGGAGTGTTCACATC	DENV2-2/pMW119	
D2_5430nt_Rv	TCGAGTTGAAATGTATCCTCTAGC		
D2_5416nt_Fw	TACATTTCAACTCGAGTAGAGATGGGTG	DENV2-3/pMW119	
D2_7889nt_Rv	CCTCCTTTTGTTAGGCCTTTGACTTC		
D2_7875nt_Fw	CCTAACAAAAGGAGGGCCAGGAC	DENV2-4/pMW119	
D2_10723nt_Rv	AGAACCTGTTGATTCAACAGCA		

Table 2. Primer list for the mutation of the DENV2 infectious clones

mutation		Sequence 5'->3'	Template	DENV2/pMW119 insertion site
prM M37I	Fw	CCCTCATTGCCATGGACCTTGGT	DENV2-1/pMW119	Sac I-BamH I
	Rv	CCATGGCAATGAGGGTACACATG		
NS4A C87S	Fw	GAATGTGCAGCATAATCACGGC	DENV2-3/pMW119	Xho I-Stu I
	Rv	TTATGCTGCACATTCCCAGAGTCATTTTTC		
NS4B A119S	Fw	CACATTATTCTATCATAGGGCCAGGAC	DENV2-3/pMW119	Xho I-Stu I
	Rv	TGATAGAATAATGTGCTACCAATAAAAGAAGG		
NS4B T244I	Fw	GAACACAATCAACACAAGAAGGGGAAC	DENV2-3/pMW119	Xho I-Stu I
	Rv	GTGTTGATTGTGTTCTTCATGATGG		
E S186F	Fw	CGGCCAGTGAATTCGAGCTCGGTAC	DENV2-1/pMW119	Sac I-BamH I
	Rv	TCTCGGAAAGCACTCCATCGTGAC		
	Fw	GAGTGCTTTCCGAGAACGGGCCT		
	Rv	CTCCTCCCAGGGATCCAAAATCCCAG		
NS1 L206P	Fw	CTGGGATTTTGGATCCCTGGGAGGAGTG	DENV2-2/pMW119	BamH I-Xho I
	Rv	GTCATTAGGCGCGCTTTCTATCCAA		
	Fw	AGCGCGCCTAATGACACATGG		
	Rv	CCCATCTCTACTCGAGTTGAAATGTAT		
NS1 N246D	Fw	CTGGGATTTTGGATCCCTGGGAGGAGTG	DENV2-2/pMW119	BamH I-Xho I
	Rv	GCAAAATCCTTTGGAATTATCATCTCA		
	Fw	TCCAAAGGATTTTGCTGGACCAGTAT		
	Rv	CCCATCTCTACTCGAGTTGAAATGTAT		
NS5 V130A	Fw	TAACCTTAGCGACCGGGCCCATTTCCACATTG	DENV2-4/pMW119	Apa I-Apa I
	Rv	AACGTCAGCTCCACTTTGAAGACGCA		
	Fw	AGTGGAGCTGACGTTTTCTTTACC		
	Rv	CTTCATCCCACCTTGGGCCCCCATTGTTGC		

Replicon assay

The DENV2 replicon plasmid, DENV2-nanoLuc/pMW119 was generated based on DGL2[29]. The reporter gene was recombined from Gaussia luciferase to nanoLuc and DENV1 genomic sequence was recombined into DENV2 genomic sequence. DENV2-nanoLuc/pMW119 and pGL4.54 (Promega Corporation, Madison, WI, USA) were co-transfected into BHK-21 cells using Lipofectamine 3000 (Thermo Fisher Scientific). At 4 hours post transfection (hpt), cells were re-seeded into a 384-well plate, including each concentration of compound. At 72 hpt, nanoLuc and firefly lucicferase (fLuc) activity were measured using the Nano-Glo Dual-Luciferase Reporter Assay System (Promega Corporation), and the EC_{50} was calculated using the two-point method. These assays were performed in duplicate and repeated three times.

Total cellular RNA extraction and quantitative reverse transcription PCR (RT-qPCR)

DENV2-infected BHK-21 or A549 cells were washed with phosphate-buffered saline (PBS) and lysed with RNA lysis buffer [4 M guanidine thiocyanate, 10 mM Tris(hydroxymethyl)aminomethane hydrochloride (Tris-HCl) (pH 7.5), 1% 2-mercaptoethanol; 100 μL/well]. Cell lysis solutions were passed through a Wizard SV96 DNA binding plate (Promega Corporation) by vacuum suction. The binding plate was washed with RNA wash solution [60 mM potassium acetate, 10 mM Tris-HCl (pH 7.5), 60% ethanol; 1 mL/well] and the RNA was eluted with double-distilled water (100 μL/well). RT-qPCR was performed using the EXPRESS One-Step SuperScript qRT-PCR kit, universal (Thermo Fisher Scientific). The primer sets for DENV2, glyceraldehyde-3-phosphate dehydrogenase (GAPDH), and Actin Beta (ACTB) (VIC-MGB 4448489) were purchased from Life Technologies. The primer and probe sequence for DENV2 and GAPDH were DENV2_Fw (5'-AGT GGA CAC GAG AAC CCA AGA-3'), DENV2_Rv (5'-TTC GGC CGT GAT TTT CAT TAG-5'), DENV2_probe (5'-FAM-AAA AGA AGG CAC GAA GAA-MGB-3'), BHK_GAPDH_Fw (5'-GGT CGG AGT GAA CGG ATT TG-3'), BHK_GAPDH_Rv (5'-AGT GAA GGC AGC CCT GGT AA-3'), and BHK_GAPDH_probe (5'-VIC-CCG TAT TGG ACG CCT G-MGB-3'). DENV2 RNA copies were normalized to GAPDH mRNA copies for BHK-21 cells and ACTB for A549 cells. Antiviral activity of compounds was measured 48 hours post-infection (hpi) for BHK-21 cells and 72 hpi for A549 cells and the EC_{50} or 90% effective concentration (EC_{90}) were calculated using the two-point method.

Plaque titration and cloning

Plaque titration and cloning were performed using BHK-21 cells. For plaque titration, the cells were incubated with diluted DENV for 1 h, washed with PBS, combined with 1% methylcellulose EMEM containing 2% FBS, and incubated for 4 days. The methylcellulose medium was removed and Masked Form A (pH 7.2–7.6) (Japan Tanner Co., Osaka, Japan) was added to cell fixation. After washing with PBS, the cells were stained with 0.1% crystal violet. Plaque cloning was performed as described above. After DENV infection, the cells were overlaid with RPMI 1640 medium containing 4% FBS and 0.9% SeaPlaque agarose (Lonza, Basel, Switzerland) and incubated for 5 days. Afterward, the cells were stained by incubation with MTT at 37 °C for 4 h. Single colonies were collected with a pipet and used for inoculation of BHK-21 cells to obtain cloned viruses.

Sequence alignment analysis of the NS1, NS4A, and NS5 MTase domain of flavivirus

The amino acid sequence of the NS1, NS4A, and NS5 MTase domain coding region of DENV1–4 was estimated from genome sequences obtained in my laboratory. The sequences of JEV, WNV, YFV, and ZIKV were downloaded from the GenBank database (https://www.ncbi.nlm.nih.gov/genbank/). Multiple alignment analysis was performed with GENETYX software v. 11 (Genetyx Corporation, Tokyo, Japan).

DENV2 MTase assay

The DENV2 MTase assay was performed using a modification of a previously reported method[30, 31]. Recombinant MTase plasmid, contained in the pGEX-6P-1 vector (GE Healthcare, United Kingdom), was expressed in BL21 (DE3) pLysS competent cells (Stratagene, La Jolla, CA, USA), and purified using a GSTPrap FF column (GE Healthcare). Briefly, BL21 (DE3) pLysS competent cells transformed with the expression plasmid were grown in LB at 37 °C to 0.6~0.8 O.D. at 600 nm, induced with 0.4 mM isopropyl-β-D-thiogalactopyranoside (IPTG) at 16 °C overnight, and harvested by centrifugation. Cell pellets were resuspended and sonicated in Buffer A [20 mM Tris-HCl (pH 7.5), 200 mM sodium chloride, 2 mM β-mercaptoethanol, 10% glycerol] plus lysozyme, DNase and a protease inhibitor cocktail. After centrifugation, the lysate supernatant was loaded onto a GSTPrap FF column. The GST tag was cleaved 4 h at 4 °C by PreScission protease and the DENV MTase was eluted with Buffer A. The eluted protein was exchanged from Buffer A to Buffer B [50 mM Tris-HCl (pH 7.5), 40% glycerol, 1 mM dithiothreitol (DTT)] by using a HiTrap Desalting column (GE Healthcare). The protein was further concentrated using an Amicon Ultra tube (Millipore,

Billerica, MA).

The RNA substrate used for the MTase assay was a 200 nt DENV2 5'-untranslated region (UTR) RNA. The DENV2 cDNA template was prepared by reverse transcription using SuperScript III Reverse Transcriptase (Invitrogen) with the genomic RNA of DENV2 and a random hexamer. The reverse transcription reaction mixture was used as a template for PCR amplification using a 200 nt DENV2 5'-UTR RNA segment. The PCR product of the 200 nt DENV2 5'-UTR RNA segment was generated by using the following primers: T7_DENV2_1-17nt_Fw: 5'-CAG TAA TAC GAC TCA CTA TTA GTT GTT AGT CTA CGT G-3', DENV2_200-174nt_Rv: 5'-AGT GAG AAT CTC TTT GTC AAC TGT TGC-3'. DENV2 5'UTR 200 nt RNA was generated using a MEGAshortscript T7 Transcription Kit (Invitrogen) from the PCR product. *In vitro* synthesized RNA was capped using [α-^{32}P] guanosine triphosphate (GTP) (PerkinElmer) and a vaccinia virus capping enzyme (Cellscript, Madison, WI) in the absence or presence of cold S-adenosyl-L-methionine (SAM) according to the manufacturer′s instructions. The resulting 5′-labeled G[^{32}-P] pppA and m7G[^{32}-P] pppA-RNA were used as substrates for N-7 and 2′-O methylations, respectively. For the removal of unincorporated [α-^{32}P] GTP, the capping reactions were passed through a Micro Bio-Spin 30 Column (Bio-Rad Laboratories, Hercules, CA, USA).

The N-7 methylation was performed in assay buffer containing 50 mM Tris-HCl (pH 7.5), 20 mM sodium chloride, GTP capped 200 nt DENV2 5'-UTR RNA, 0.2 μM SAM, and 400 nM MTase at 30 °C for 20 minutes (min). The 2′-O methylation was performed in assay buffer containing 50 mM Tris-HCl (pH 7.5), 10 mM potassium chloride, 2 mM magnesium chloride, 1 mM DTT, m7GTP capped 200 nt DENV2 5'-UTR RNA, 0.2 μM SAM and 400 nM MTase at 30 °C for 60 min. All methylation reactions were stopped by incubation at 95 °C for 5 min followed by purification using a Micro Bio-Spin 30 Column. The reaction products were digested with nuclease P1 overnight and analyzed on polyethyleneimine cellulose thin-layer chromatography (TLC) plates (Millipore, Billerica, MA, USA) using 0.45 M ammonium sulfate as the solvent. The radioactive cap structure separated on the TLC plates was quantified by BAS-2500 (Fujifilm, Japan).

Results

Compound screening for anti-DENV2 activity and identified three novel anti-DENV2 compounds

A screening system based on a DENV-infected cell-based assay was developed to identify novel low-molecular-weight compounds with anti-DENV activities. DENV2-infected BHK-21 cells were used for this assay, because a CPE consisting of rounding of the cells was observed and these cells were unresponsive to the MTT reagent. The antiviral activity was measured with the MTT assay using cell damage associated with viral infection as an index. MTT assay conditions were optimized using ribavirin and mycophenolic acid, which have established anti-DENV activities *in vitro*[32]. After screening of about 7,000 compounds from the compound library for anti-DENV activity, Compound-B which possess a benzimidazole skeleton (Figure 1A) and Compound-X and Compound-Y, which have quinolone skeleton (Figure 1B and 1C) were found.

The EC_{50} of Compound-B against DENV2 was 1.32 μM, and a slight cell cytotoxicity was observed (CC_{50} = 13.5 μM) (Table 3). Compound-B was also effective against the three other serotypes of DENV, DENV1, 3, and 4, with EC_{50}s of 1.81 μM, 2.66 μM, and 4.12 μM, respectively. Moreover, Compound-B also showed anti-DENV2 activity in human cell line; A549 cells. In the additional assays using DENV2 replicon, Compound-B effectively inhibited DENV2 subgenomic replication. Next, the antiviral activities of Compound-B against the flaviviruses including WNV, JEV, YFV, and ZIKV were investigated; however, no antiviral activities against these flaviviruses were observed up to 18.9 μM (data not shown). These results suggest that the antiviral activity of Compound-B is specific for DENV.

The EC_{50}s of Compound-X and Compound-Y against DENV2 were 3.88 μM and 9.19 μM, respectively (Table 4). No cytotoxicity was observed even at the highest concentration of 50 μM for both compounds. The viral RNA reduction assay using A549 cells revealed that both Compound-X and Compound-Y had anti-DENV2 activities with EC_{50}s of 3.33 μM and 5.28 μM, respectively. To clarify whether the quinolone compounds inhibit viral replication, a DENV2 subgenomic replicon was applied to examine the suppression effect of these compounds by measurement of gene expression of a reporter gene. Compound-X and Compound-Y showed a concentration-dependent inhibition at 72 hpt of DENV2 replicon plasmids with EC_{50} of 27.7 μM and 20.9 μM, respectively. Although the efficacies of Compound-X and Compound-Y were reduced compared with those observed by the MTT assay, virus replication inhibitory activity was observed. These quinolone compounds were equally effective against DENV1 but less effective

against DENV3 and DENV4, and the EC_{50}s of Compound-X were 4.58 μM, 10.9 μM, and 13.3 μM, and Compound-Y were 4.94 μM, >50 μM, and 21.6 μM, against DENV1, DENV3, and DENV4, respectively (Table 5). Furthermore Compound-X was effective against other flaviviruses, including ZIKV, JEV, and WNV but not YFV; however, Compound-Y was not effective against the other flaviviruses.

Isolation of compound-resistant DENV2 clones

To identify the target sites of Compound-B, Compound-X, and Compound-Y, DENV2 was cultured in the presence of the compounds to generate resistant viruses.

Compound-B-resistant DENV2 were isolated after 20 days incubation in the presence of Compound-B (3.4–6.8 μM). Three DENV2-resistant clones were obtained by plaque cloning. The plaque sizes of these three clones were smaller than that of passaged-DENV2 (Figure 2). To measure the fold resistance of these clones to Compound-B, an MTT assay was conducted. With the same MOI, the efficacies of ribavirin and mycophenolic acid against these three clones were almost comparable with that of the passaged-DENV2. In contrast, compared with the passaged-DENV2, the three isolated clones were resistant to Compound-B by 2.40–3.05-fold (Table 6).

The Compound-X-resistant DENV2 was isolated after incubation with Compound-X at 11.8 μM for 10 days followed by 23.7 μM for 20 days. Compound-Y-resistant DENV2 was isolated in a similar manner as Compound-X where DENV2 was incubated with Compound-Y at 11.0 μM for 10 days followed by 22.0 μM for 20 days. Subsequently three clones of each were obtained by plaque cloning. The efficacy of each compound against each isolated resistant DENV2 sample was measured using the MTT assay. Ribavirin and mycophenolic acid showed almost the same efficacy against the compound-resistant DENV2 and passaged-DENV2 (Table 7). The drug sensitivity was reduced 2.86 to 4.11 times for Compound-X against Compound-X-resistant DENV2 compared with passaged-DENV2, and 2.91 to 3.25 times for Compound-Y against Compound-Y-resistant DENV2 compared with passaged-DENV2. Notably Compound-X and Compound-Y-resistant viruses also exhibited cross-resistance to each other. For example, drug sensitivity was reduced 3.22 to 3.98 times for Compound-X against Compound-Y-resistant DENV2 compared with passaged-DENV2 and 2.41 to 2.97 times for Compound-Y against Compound-X-resistant DENV2 compared with passaged-DENV2.

Table 3. Efficacy of Compound-B against DENV in the MTT assay, RT-qPCR assay, and subgenomic replicon assay and cell toxicity

Data represent mean values ± Standard deviation (SD) of at least three independent experiments.

	BHK-21 MTT				
	EC_{50} (μM)				CC_{50} (μM)
	DENV2	DENV1	DENV3	DENV4	
Compound-B	1.32 ± 0.19	1.81 ± 0.15	2.66 ± 0.08	4.12 ± 0.15	13.5 ± 3.1
Ribavirin	26.6 ± 0.6	31.8 ± 1.6	60.3 ± 1.7	100 ± 4	> 400
Mycophenolic acid	0.123 ± 0.004	0.127 ± 0.001	0.139 ± 0.001	0.253 ± 0.008	> 3

	A549 RT-qPCR	BHK-21 replicon
	EC_{50} (μM)	EC_{50} (μM)
	DENV2	DENV2
Compound-B	1.84 ± 0.15	3.10 ± 1.47
Ribavirin	99.9 ± 42.8	36.4 ± 6.3
Mycophenolic acid	0.191 ± 0.007	0.189 ± 0.072

Table 4. Efficacy of Compound-X and Compound-Y against DENV2 in the MTT assay, RT-qPCR assay, and subgenomic replicon assay and cell toxicity

Data represents the mean value ± SD of at least three independent experiments. NT: Not tested.

	BHK-21 MTT	A549 RT-qPCR	BHK-21 replicon	BHK-21 MTT
	EC_{50} (μM)	EC_{50} (μM)	EC_{50} (μM)	CC_{50} (μM)
Compound-X	3.88 ± 1.10	3.33 ± 0.50	27.7 ± 2.2	>50
Compound-Y	9.19 ± 3.19	5.28 ± 0.23	20.9 ± 2.1	>50
Ribavirin	40.2 ± 2.4	21.2 ± 0.9	66.5 ± 1.0	>400
Mycophenolic acid	0.125 ± 0.011	NT	NT	>3

Table 5. Efficacy of Compound-X and Compound-Y against DENV1, 3, and 4 and other flaviviruses in the MTT assay

Data represents the mean value ± SD of at least three independent experiments.

	EC_{50} (μM)		
	DENV1	DENV3	DENV4
Compound-X	4.58 ± 1.58	10.9 ± 1.6	13.3 ± 2.9
Compound-Y	4.94 ± 2.68	> 50	21.6 ± 0.9
Ribavirin	27.0 ± 4.1	50.5 ± 5.6	49.0 ± 8.7
Mycophenolic acid	0.174 ± 0.060	0.169 ± 0.051	0.175 ± 0.060

	EC_{50} (μM)			
	ZIKV	JEV	WNV	YFV
Compound-X	16.7 ± 1.5	12.3 ± 1.4	10.3 ± 0.4	>50
Compound-Y	>50	>50	>50	>50
Ribavirin	41.5 ± 1.8	32.5 ± 2.0	20.9 ± 2.0	31.2 ± 3.3

A

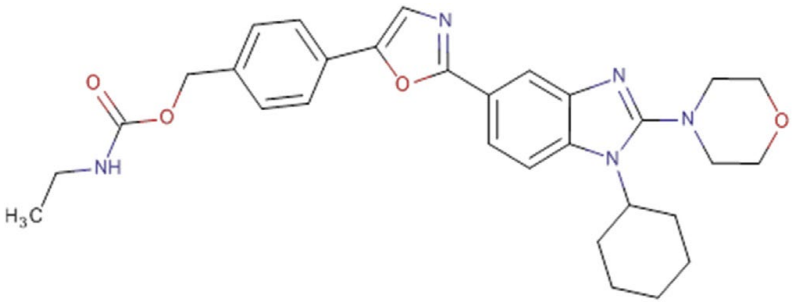

B

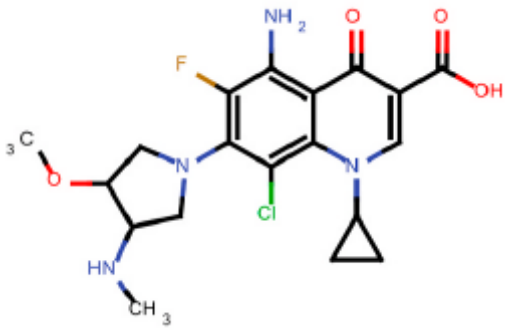

C

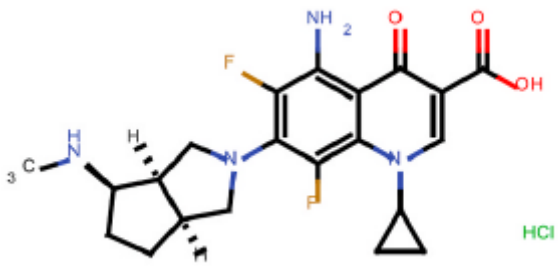

Figure 1. Chemical structure of compounds

(A) Compound-B, (B) Compound-X, and (C) Compound-Y.

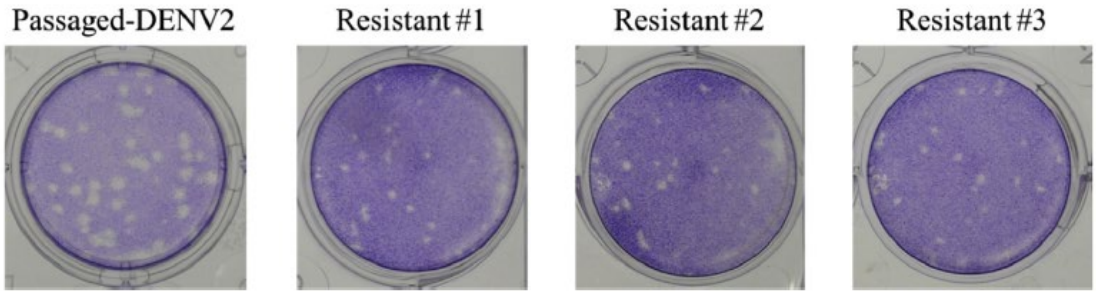

Figure 2. Plaque sizes after infection with passaged-DENV2 and Compound-B-resistant DENV2

Passaged-DENV2 and Compound-B-resistant DENV2 #1–3 were infected to BHK-21 cells and plaque titration was performed. The cells were stained with crystal violet.

Table 6. Efficacy of the compounds against Compound-B-resistant DENV2

Data represent mean values ± SD of at least three independent experiments. FR: Fold resistance v.s. passaged-DENV2.

		Passaged-DENV2	Compound-B-resistant DENV2		
			#1	#2	#3
Compound-B	EC_{50} (μM)	2.79 ± 0.12	8.07 ± 0.69	8.50 ± 0.49	6.67 ± 0.04
	FR	-	2.90	3.05	2.40
Ribavirin	EC_{50} (μM)	34.9 ± 2.9	30.8 ± 3.5	31.7 ± 3.9	28.7 ± 5.1
	FR	-	0.88	0.91	0.82
Mycophenolic acid	EC_{50} (μM)	0.126 ± 0.01	0.120 ± 0.01	0.119 ± 0.01	0.115 ± 0.01
	FR	-	0.95	0.95	0.92

Table 7. Efficacy of the compounds against Compound-X-resistant DENV2 and Compound-Y-resistant DENV2

Data represents the mean value ± SD of at least three independent experiments. FR: Fold resistance versus passaged-DENV2.

		Passaged-DENV2	Compound-X-resistant DENV2		
			#1	#2	#3
Compound-X	EC_{50} (μM)	6.98 ± 1.41	19.5 ± 2.4	21.5 ± 0.1	28.7 ± 5.8
	FR	–	2.86	3.25	4.11
Compound-Y	EC_{50} (μM)	10.6 ± 0.5	25.6 ± 2.1	28.3 ± 0.3	31.7 ± 4.6
	FR	–	2.41	2.67	2.97
Ribavirin	EC_{50} (μM)	39.5 ± 4.9	35.2 ± 3.6	36.5 ± 1.8	39.7 ± 5.5
	FR	–	0.89	0.93	1.00
Mycophenolic acid	EC_{50} (μM)	0.124 ± 0.006	0.124 ± 0.008	0.125 ± 0.005	0.124 ± 0.003
	FR	–	1.00	1.01	1.00

		Compound-Y-resistant DENV2		
		#1	#2	#3
Compound-X	EC_{50} (μM)	27.5 ± 4.7	23.8 ± 2.6	22.2 ± 3.7
	FR	3.98	3.50	3.22
Compound-Y	EC_{50} (μM)	34.5 ± 1.4	30.9 ± 1.9	34.2 ± 4.3
	FR	3.25	2.91	3.21
Ribavirin	EC_{50} (μM)	41.5 ± 4.9	36.9 ± 2.9	37.2 ± 2.6
	FR	1.05	0.93	0.94
Mycophenolic acid	EC_{50} (μM)	0.122 ± 0.002	0.124 ± 0.004	0.123 ± 0.001
	FR	0.98	1.00	0.99

Genome analysis of compound-resistant DENV2

Full genome analysis was performed using Ion PGM to identify mutation sites in the compound-resistant DENV2 samples.

Several amino acid substitutions in the three Compound-B-resistant DENV2 clones were identified. All three clones carried cystatin-to-serine at amino acid position 87 (C87S) in NS4A; one clone carried the mutations methionine-isoleucine at amino acid position 37 (M37I) in prM, alanine-to-serine at amino acid position 119 (A119S) in NS4B, or threonine-to-isoleucine at amino acid position 244 (T244I) in NS4B (Table 8). Other mutations were confirmed threonine-to-lysine at amino acid position 120 (T120K) in E and tyrosine-to-cysteine at amino acid position 97 (Y97C) in NS4A proteins; however, these mutations were also observed in the passaged-DENV2.

The isolated Compound-X-resistant DENV2 and Compound-Y-resistant DENV2 contained multiple mutations. Among these mutations common to Compound-X-resistant and Compound-Y-resistant DENV2 were serine-to-phenylalanine at amino acid position 186 (S186F) in E and valine-to-alanine at amino acid position 130 (V130A in NS5 (Table 9). Three amino acid substitutions, T120K in E, methionine-to-threonine at amino acid position 85 (M85T) in NS4A, and glycine-to-alanine at amino acid position 124 (G124A) in NS4B, were also found in passaged-DENV2. In terms of the noncommon mutations, asparagine-to-aspartic acid at amino acid position 246 (N246D) in NS1 was found in Compound-X-resistant DENV2, leucine-to-proline at amino acid position 206 (L206P) in NS1 was found in Compound-Y-resistant DENV2, and methionine-to-valine at amino acid position 196 (M196V) in E was found in one clone of Compound-Y-resistant DENV2.

The NS4A C87S mutation was resistant to Compound-B

Since some mutations in prM, NS4A, and NS4B were observed in Compound-B-resistant DENV2, infectious DENV2 clones with single amino acid substitutions were constructed. Then, viral growth at the cellular viral RNA level and the plaque size of the mutant strains were compared with that of the wild-type (WT) strain. The cellular viral RNA levels of each substituted infectious clone were measured every 12 h until 72 hours post-infection (hpi) (Figure 3A). The viral RNA levels increased until 60 hpi following development of a CPE. The viral proliferations of the prM M37I and NS4B A119S mutant strains at the viral RNA level were similar to that of the WT strain. In contrast, the viral proliferation of the NS4A C87S and NS4B T244I mutant strains was lower than that of the WT strain at all time points. Notably at the viral RNA level, expression of the NS4A C87S mutant strain was less than a quarter of that of the WT strain at 48 hpi. The plaque

sizes of the prM M37I, NS4B A119S, and NS4B T244I mutant strains were almost the same as that of the WT strain, while the plaque size of the NS4A C87S mutant strain was slightly smaller than that of the WT strain (Figure 3B). Analyses of the cellular viral RNA level and plaque size showed that the NS4A C87S mutant strain had the slowest proliferation rate among the WT and other mutant strains.

Because the NS4A C87S mutant strain proliferation was markedly reduced, the susceptibility of each mutant strain with a single amino acid substitution and the WT strain to Compound-B was incompatible with examination by MTT assay. Therefore, the antiviral activity of Compound-B against each DENV2 mutant strain with a single amino acid substitution was measured based on the cellular viral RNA levels using BHK-21 cells. The efficacy of ribavirin, used as a reference compound, against these mutant strains was comparable. Compound-B had the same efficacy against the prM M37I and NS4B A119S mutant strains, and a slightly lower efficacy against the NS4B T244I mutant strain (1.71-fold) (Table 10). Most importantly, among all mutant strains with a single amino acid substitution, the NS4A C87S mutant strain had the highest resistance to Compound-B (3.02-fold). Together, these results demonstrated that the NS4A C87S mutation was the primary cause of resistance to Compound-B and that the target region of Compound-B is the C87 of the viral NS protein NS4A.

Table 8. Amino acid mutations in Compound-B-resistant DENV2

Viral protein		prM	E	NS4A			NS4B	
Residue and position		M37	T120	M85	C87	Y97	A119	T244
Passaged-DENV2		M	**K**	**T**	C	**C**	A	T
Compound-B-resistant DENV2	#1	M	**K**	**T**	**S**	Y	A	T
	#2	M	**K**	M	**S**	**C**	A	T
	#3	**I**	**K**	M	**S**	Y	**S**	**I**

Table 9. Amino acid mutations in Compound-X-resistant DENV2 and Compound-Y-resistant DENV2

Viral protein		E			NS1		NS4A	NS4B	NS5
Residue and position		T120	S186	M196	L206	N246	M85	G124	V130
Passaged-DENV2		**K**	S	M	L	N	**T**	**A**	V
Compound-X-	#1	**K**	**F**	M	L	**D**	**T**	**A**	**A**
resistant	#2	**K**	**F**	M	L	**D**	**T**	**A**	**A**
DENV2	#3	**K**	**F**	M	L	**D**	**T**	**A**	**A**
Compound-Y-	#1	**K**	**F**	**V**	**P**	N	**T**	**A**	**A**
resistant	#2	**K**	**F**	M	**P**	N	**T**	**A**	**A**
DENV2	#3	**K**	**F**	M	**P**	N	**T**	**A**	**A**

A

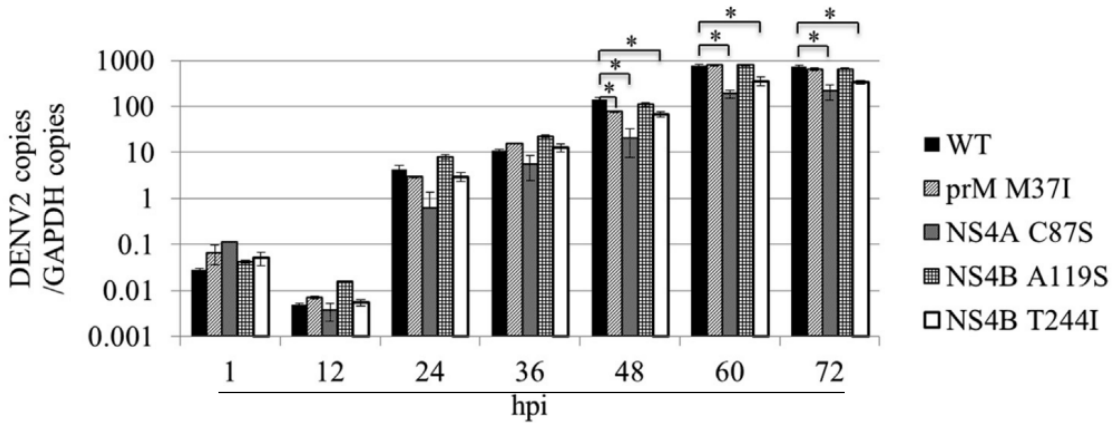

B

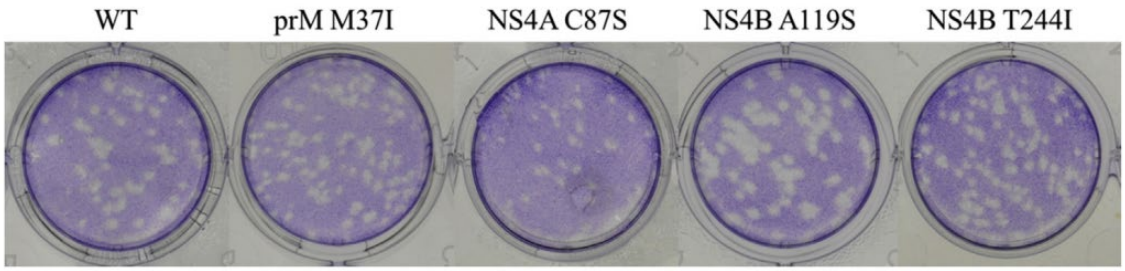

Figure 3. Analysis of viral proliferation of the single amino acid substitutions associated with Compound-B-resistant DENV2

(A) Cellular viral RNA of single amino acid substitutions of DENV2 infectious clones at 1, 12, 24, 36, 48, 60, and 72 hpi. DENV2 RNA copies were normalized to GAPDH mRNA copies. Data represent mean values ± SD of at least three independent experiments. Significance was analyzed by the Student's *t*-test and indicated by asterisks (* $P < 0.05$). (B) Plaque sizes after infection with DENV2 infectious clones with single amino acid substitutions. The cells were stained with crystal violet.

Table 10. Efficacy of Compound-B against the single amino acid substitutions of DENV2 infectious clones

Data represent mean values ± SD of at least three independent experiments. FR: Fold resistance v.s. WT.

		WT	prM M37I	NS4A C87S	NS4B A119S	NS4B T244I
Compound-B	EC_{50} (μM)	1.02 ± 0.05	1.51 ± 0.12	4.01 ± 0.37	1.40 ± 0.05	2.07 ± 0.06
	EC_{90} (μM)	2.52 ± 0.31	2.86 ± 0.45	7.60 ± 0.29	3.01 ± 0.03	4.30 ± 0.25
	FR of EC_{90}	–	1.13	3.02	1.14	1.71
Ribavirin	EC_{50} (μM)	8.72 ± 0.81	10.1 ± 0.7	14.1 ± 1.6	15.9 ± 1.3	13.4 ± 0.7
	EC_{90} (μM)	40.3 ± 10.5	35.1 ± 1.7	42.5 ± 3.4	36.4 ± 4.2	39.9 ± 0.8
	FR of EC_{90}	–	0.87	1.05	0.90	0.99

The NS5 V130A mutation in a DENV2 infectious clone moderately contributed to resistance against Compound-X and Compound-Y

Since multiple mutations were observed in Compound-X-resistant and Compound-Y-resistant DENV2, infectious DENV2 clones with single amino acid substitutions were constructed. NS1 N246D and NS1 L206P mutations were observed in Compound-X-resistant DENV2 and Compound-Y-resistant DENV2, respectively, therefore, each mutation was combined with NS5 V130A to construct two double mutants. The antiviral activity of the DENV2 clones with each mutation was measured using the MTT assay. The drug sensitivity of each single mutation clone, E S186F, NS1 L206P, and NS1 N246D showed almost no change toward Compound-X and Compound-Y compared to WT (Table 11). The NS5 V130A mutation had a slight effect on drug sensitivity, as the efficacy of Compound-X was reduced by 1.42 times, and Compound-Y was reduced by 1.53 times compared with WT. Furthermore, for the NS1 N246D/NS5 V130A double mutant, the sensitivity was further reduced by 2.76 times for Compound-X and 2.71 times for Compound-Y compared to WT. In comparison, the efficacies of Compound-X and Compound-Y were not further reduced when tested against the NS1 L206P/NS5 V130A double mutants. In addition, the cellular viral RNA levels of each substituted infectious clone were measured every 24 h until 72 hpi (Figure 4). Viral replication of each infectious clone containing a single mutation (E S186F, NS1 L206P, NS1 N246D, and NS5 V130A) were lower at the RNA level than that of the WT strain. The viral proliferation of the NS1 L206P/NS5 V130A double mutant clone was also lower than the WT strain. In contrast, the viral proliferation of the NS5 V130A/NS1 N246P double mutant strain was slightly higher than that of WT strain.

Table 11. Efficacy of Compound-X and Compound-Y against the DENV2 infectious clones containing amino acid substitutions

Data represents the mean value ± SD of at least three independent experiments. FR: Fold resistance versus passaged-DENV2.

		WT	E S186F	NS1 L206P	NS1 N246D
Compound-X	EC_{50} (μM)	10.9 ± 2.0	7.94 ± 0.51	9.40 ± 2.61	11.4 ± 2.2
	FR	–	0.74	0.83	1.04
Compound-Y	EC_{50} (μM)	17.0 ± 1.8	14.0 ± 0.8	13.9 ± 3.0	17.0 ± 2.2
	FR	–	0.82	0.80	0.99
Ribavirin	EC_{50} (μM)	50.3 ± 4.6	56.2 ± 1.4	53.5 ± 7.7	56.4 ± 6.6
	FR	–	1.12	1.05	1.11
Mycophenolic acid	EC_{50} (μM)	0.129 ± 0.005	0.141 ± 0.004	0.139 ± 0.016	0.142 ± 0.017
	FR	-	1.09	1.07	1.10

		NS5 V130A	NS1 L206P NS5 V130A	NS1 N246D NS5 V130A
Compound-X	EC_{50} (μM)	15.9 ± 4.9	12.9 ± 3.8	29.6 ± 2.7
	FR	1.42	1.16	2.76
Compound-Y	EC_{50} (μM)	26.4 ± 6.0	24.3 ± 6	46.0 ± 2.3
	FR	1.53	1.40	2.71
Ribavirin	EC_{50} (μM)	61.3 ± 4.9	52.8 ± 7.5	66.8 ± 0.9
	FR	1.22	1.04	1.33
Mycophenolic acid	EC_{50} (μM)	0.161 ± 0.031	0.138 ± 0.016	0.185 ± 0.022
	FR	1.23 ± 0.18	1.07 ± 0.07	1.43 ± 0.10

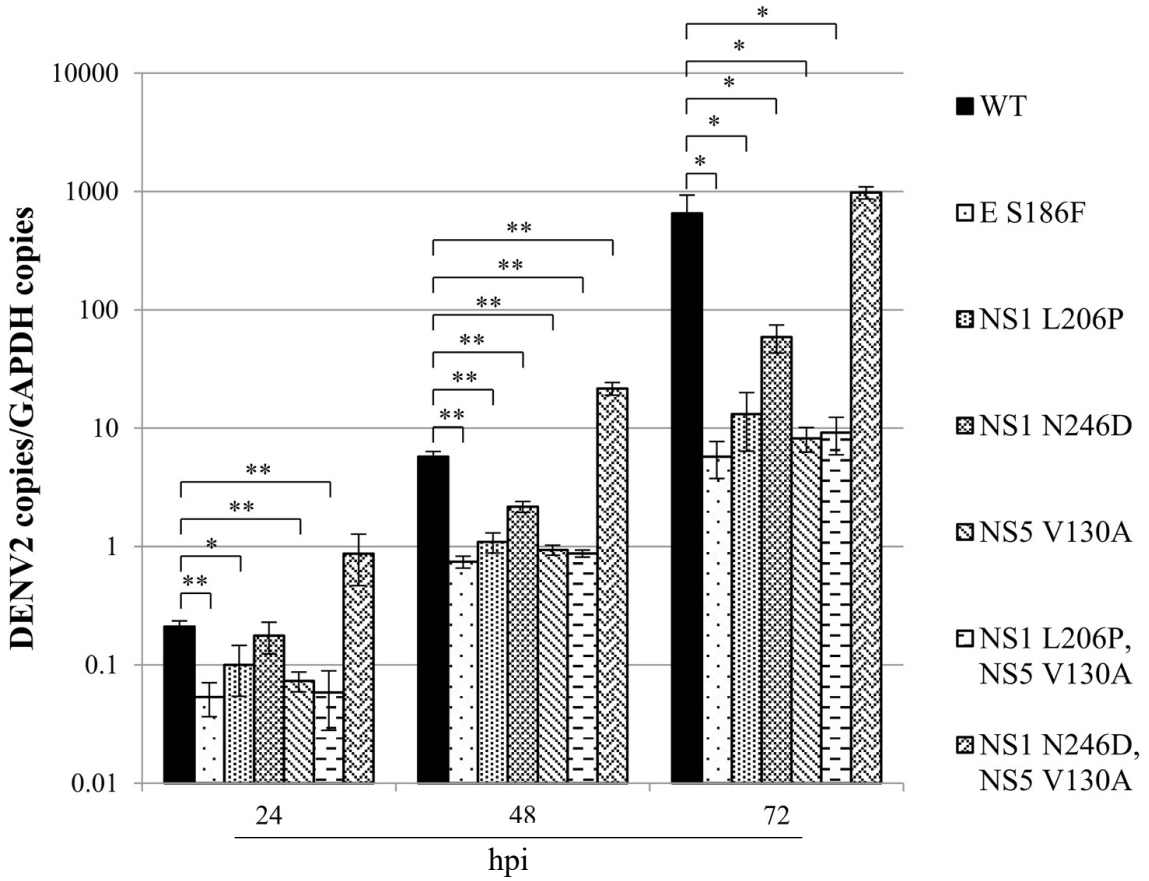

Figure 4. Analysis of the replication of DENV2 containing amino acid substitutions associated with Compound-X and Compound-Y-resistant DENV2

Cellular viral RNA from the DENV2 infectious clones containing amino acid substitutions was analyzed at 24, 48, and 72 hpi in BHK-21 cells. DENV2 RNA copies were normalized to GAPDH mRNA copies. Data represents the mean value ± SD of at least three independent experiments. Significance was analyzed by the Student's *t*-test and indicated by asterisks (*$P < 0.05$, **$P < 0.01$).

Discussion

In this study, a cell-based screening of a library of low molecular weight compounds, including anti-HCV and -HIV compounds, was conducted and Compound-B, Compound-X, and Compound-Y as potential novel anti-DENV agents were identified.

Compound-B has a benzimidazole skeleton that inhibits the HCV RdRp encoded in the NS protein NS5B[33-35]. HCV is a member of the genus *Hepacivirus*, family *Flaviviridae*, which is closely related to DENV. Therefore, it is assumed that Compound-B acts on DENV RdRp encoded in the C-terminal region of the NS protein NS5. However, the results of an RdRp inhibition assay[36] showed that Compound-B had no inhibitory activity against DENV2 RdRp (data not shown).

Compound-B-resistant DENV2 clones were isolated, and their whole genome was sequenced. In the resistant viruses, no mutation was observed in the RdRp region, whereas several mutations were observed in the E, prM, NS4A, and NS4B proteins. Subsequently, DENV2 infectious clones with single amino acid substitutions were generated, and their properties of these mutants were characterized. Comparisons of viral proliferation revealed that the NS4A C87S mutation decreased viral proliferation. Moreover, all three isolated drug resistant clones carried this mutation. In virus passage, viruses with high proliferation rates should appear, but when the viruses are cultured in presence of the compound with antiviral activity, those with reduced proliferation may appear as a result of resistance to the compound. As the NS4A C87S mutant strain had slower proliferation than the WT strain, the NS4A C87S mutation was considered highly likely to contribute to Compound-B resistance. In fact, this mutant was the most highly resistant to Compound-B. This result suggested that NS4A C87 is the target region of Compound-B.

Among the flaviviruses, NS4A protein homology is not very high. Compared with DENV2, homologies of the NS4A protein sequences of DENV1, 3, and 4 are 59%, 61%, and 66%, respectively. And homologies of NS4A protein sequences of the other flaviviruses WNV, JEV, ZIKV, and YFV compared with DENV2 are 51%, 43%, 44%, and 33%, respectively. The homology of NS4A with DENV2 is lower in other flaviviruses than in DENV1, 3, and 4, which I speculate is a possible to reason why Compound-B did not show efficacy against other flaviviruses in the MTT assay. Moreover, NS4A C87 is conserved in DENV1, 2, and 3, but not in DENV4 (Figure 5). Therefore, it is suggested that the anti-DENV activity of Compound-B against DENV4 was lower than that against the other DENVs.

NS4A is a small hydrophobic protein comprising 150 amino acids that associate

with the endoplasmic reticulum (ER) membrane through three predicted transmembrane domains (pTMDs), including pTMD1 and pTMD3 which penetrate the ER membrane, and pTMD2 which is embedded in the ER membrane. NS4A is involved in the viral replication complex by anchoring replicase components to the intracellular membranes[37]. Although some studies have investigated the function of NS4A, the role of this protein remains largely unknown. The first 50 amino acid residues at the cytosolic N-terminal domain of NS4A interact with vimentin[38, 39]. pTMD1 is the major determinant for NS4A oligomerization and related NS4A-NS4B interactions[40, 41]. pTMD3 interacts with the mitochondrial antiviral signaling (MAVS) protein and inhibits type I interferon (IFN) production through the inhibition of retinoic acid-inducible gene-I (RIG-I)-MAVS interactions and interferon regulatory factor 3 (IRF3) activation[42]. It was recently reported that 3-hydroxy-3-methylglutaryl-Coenzyme A reductase (HMGCR) co-localized with NS4A and NS3, which are viral components involved in viral replication and localized at replicative complexes[43]. However, at present, there are no reports on the function of pTMD2, in which a Compound-B-resistant mutation was observed. As pTMD2 exists in the ER lumen in part embedded in the ER membrane, it is likely that analysis of pTMD2 function will be difficult. Therefore, it is also likely that Compound-B will be useful to clarify the function of NS4A pTMD2. Future functional analysis of NS4A will help to elucidate the precise mechanism of action of Compound-B as well as to create more efficacious compounds with anti-DENV activities through inhibition of NS4A function.

Compound-X and Compound-Y both of which contain a quinolone skeleton and demonstrated inhibitory activity against DENV2 replication activity using a DENV2 replicon assay, suggesting that they at least inhibit a virus replication step. The two laboratory-generated compound-resistant DENV2 clones demonstrated cross-resistance to each other, suggesting that the mechanisms responsible for the antiviral activity of these compounds may be similar. However, the antiviral activity profiles of these two compounds were found to be different. Compound-X was effective against other serotypes of DENV and other flaviviruses, including ZIKV, JEV, and WNV but not YFV. Compound-Y was effective against DENV1 and DENV4 but not DENV3 and the other flaviviruses.

Several mutations obtained from Compound-X-resistant DENV2 and Compound-Y-resistant DENV2 were introduced into the infectious DENV2 clone, and the effect of each mutation on the sensitivity of each compound was examined. It was shown that the NS5 V130A mutation contributed the most to the decrease in sensitivity of the quinolone compounds.

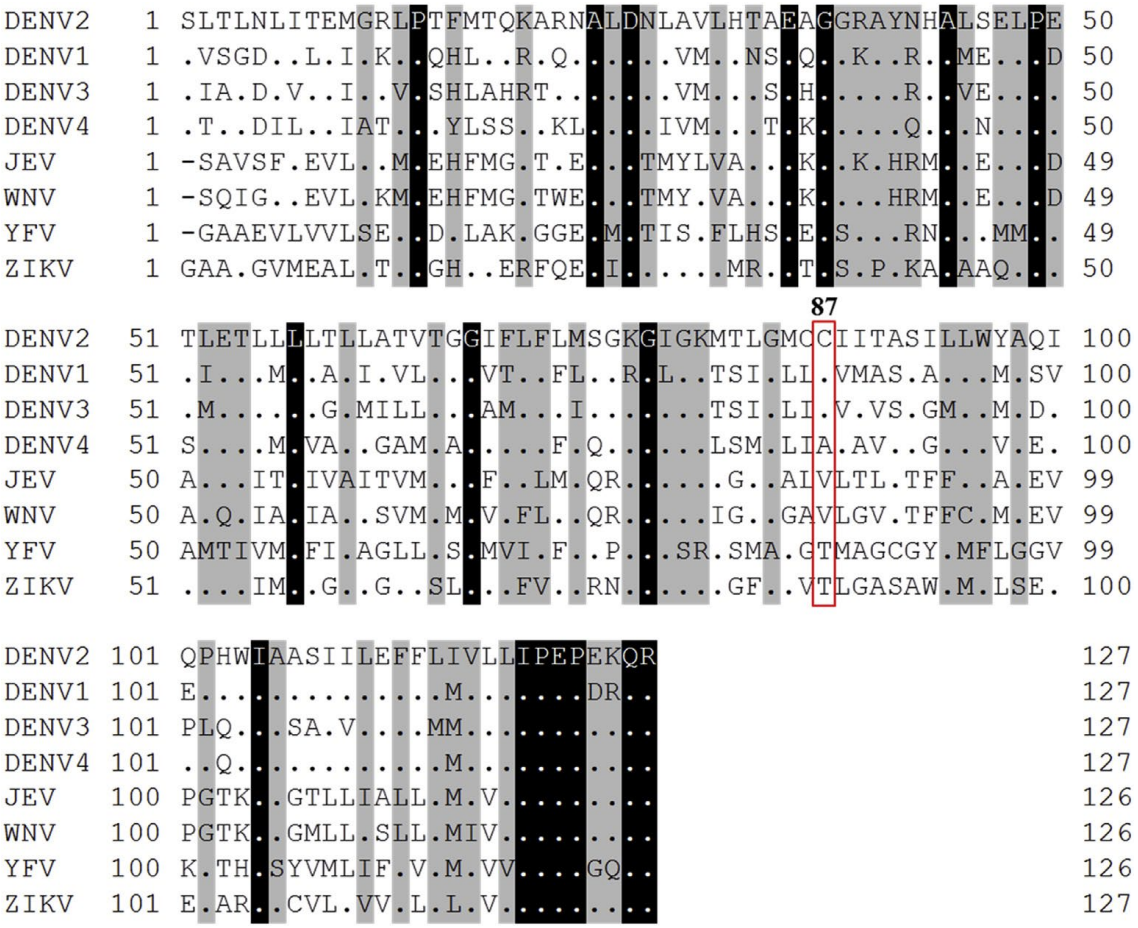

Figure 5. Amino acid sequence of flaviviruses NS4A

The black background indicates areas showed in all virus types, and the gray background is the area shared in 50% or more of viruses. The red rectangle indicates amino acid at position 87 of NS4A.

NS5 is an approximately 900 amino acid encoding protein, containing MTase and GTase domains in the N-terminal region and an RdRp domain in the C-terminal. V130 of NS5 is found in the MTase and GTase domains. The DENV genome has a guanine cap structure at the 5′-end, and the cap is methylated at its N7- and 2′O-positions. Therefore, N7- and 2′O-MTase assays using purified protein from the DENV2 MTase domain were performed following a method with minor modifications to that was previously described[30, 31]. In the N7- and 2′O-MTase enzyme inhibitory assays, sinefungin, the S-adenosylmethionine analog of the MTase substrate, showed enzyme inhibitory activity at concentrations under 1 μM. However, the quinolone compounds did not exhibit any inhibition, even at 100 μM (Figure 6A and B). The N7- and 2′ O-methylated bands were reduced at 1,000 μM by Compound-Y, but other bands were also reduced. Furthermore, I also attempted to use full-length NS5 in the MTase assay, but no MTase enzyme inhibitory activity was observed by the quinolone compounds (data not shown). Therefore, I concluded that these quinolone compounds have no direct MTase inhibitory activity in this assay. As NS5 V130 is close to the S-Adenosyl-L-homocysteine (SAH) pocket[44], I had preliminarily attempted to dock the quinolone compounds to DENV2 NS5 MTase domain. It was shown that the quinolone compounds have the possibility of binding nearby the SAH pocket (data not shown); however, the quinolone compounds did not represent MTase inhibitory activity as described above. Thus viral proteins and/or some host proteins may be needed to examine the MTase inhibitory effect by the quinolone compounds.

The valine at amino acid position 130 of NS5 is conserved in DENV2, DENV4, ZIKV, JEV, and WNV, but a lysine (K130) is present at this position in DENV1 and DENV3, and a threonine (T130) is present in YFV (red rectangle in Figure 7A). Despite these amino acid differences, the anti-flavivirus activities of Compound-X and Compound-Y were equally effective against DENV1 and DENV2, but less effective toward DENV3, DENV4, and other flaviviruses. Additionally, the results of NS5 V130A mutation analysis showed a low level of resistance towards both Compound-X and Compound-Y. Therefore, it is likely that these quinolone compounds may have antiviral activities involving other as yet unidentified amino acid residues. Incorporation of an additional NS1 N246D mutation, which is not well conserved among four serotypes of DENV, and other flaviviruses (Figure 7B), with the NS5 V130A mutation in DENV2 allowed a recovery of viral replication and further reduction of the sensitivity to the quinolone compounds, suggesting that NS1 N246 and NS5 V130 may interact. NS1 is a 352 amino acid protein that forms a dimer in DENV-infected cells[45] and is essential for viral replication with an unknown function through its interactions with NS4A and

NS4B[46, 47]. NS1 also exists as a hexamer when it is secreted extracellularly[48]. However, to date, no direct interaction between NS1 and NS5 has been reported. In this study, the MTase assay using NS5 MTase domain was performed as previously described[30, 31]. The MTase assay using only NS5 MTase domain or full-length NS5 do not exhibit enzyme inhibitory activity by the quinolone compounds in this assay. In the process of intracellular viral replication, the replication complex plays an important role, therefore, it seems to be necessary to examine MTase activity in the presence of both NS1 and NS5 proteins and possibly other viral proteins and certain host proteins. In future studies, the mechanism(s) of action responsible for the antiviral efficacy of these quinolone compounds will be investigated.

A

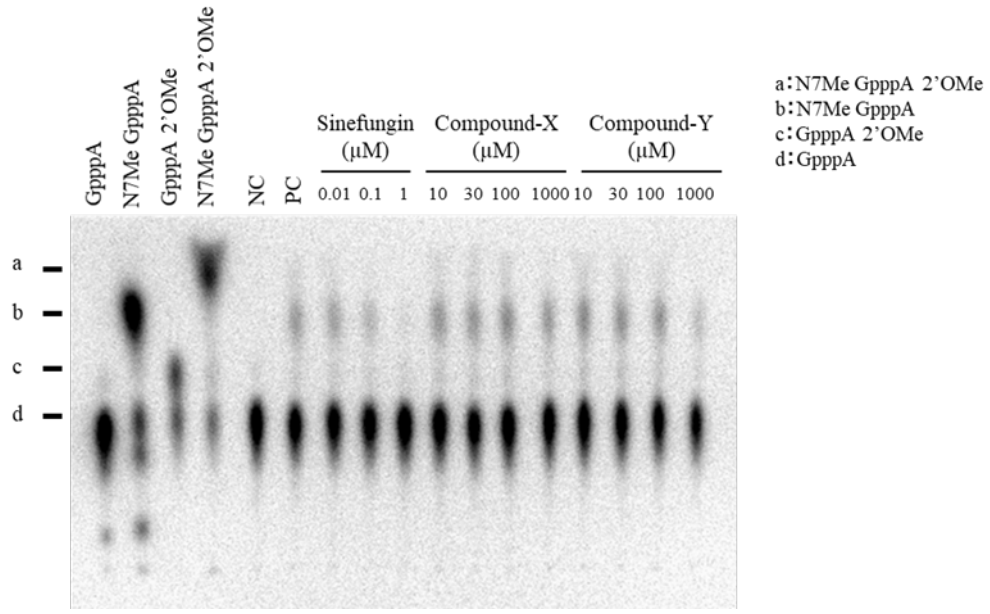

B

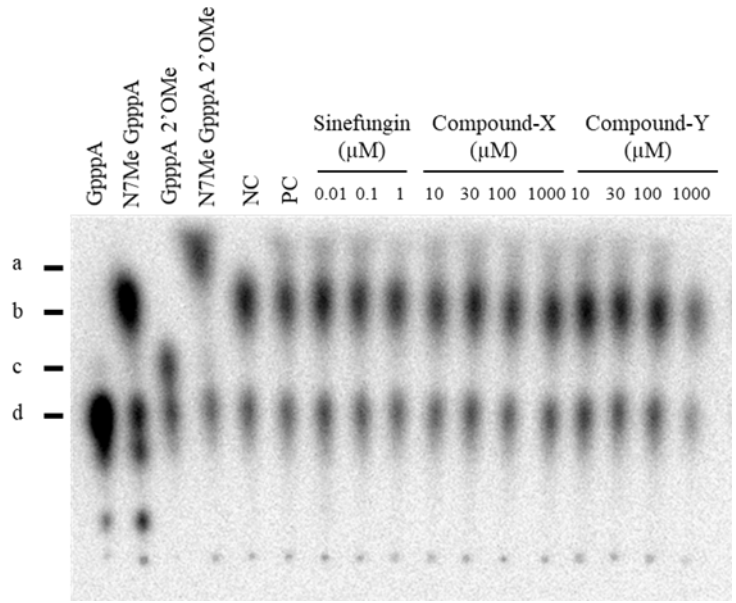

Figure 6. DENV2 MTase activity inhibitory assay using Compound-X and Compound-Y

DENV2 MTase assay using TLC plate for (A) N7 methylation and (B) 2'-O methylation. NC or PC means negative control or positive control for each reaction.

A

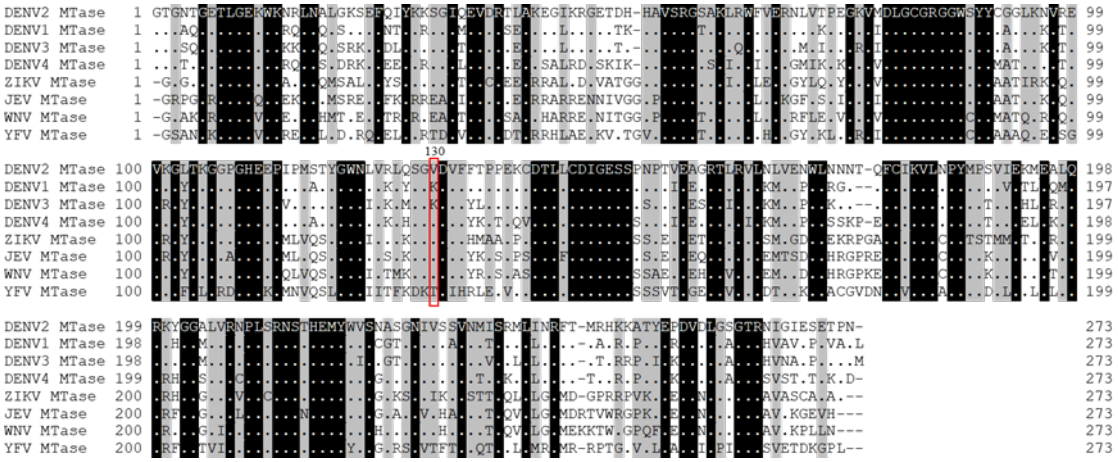

B

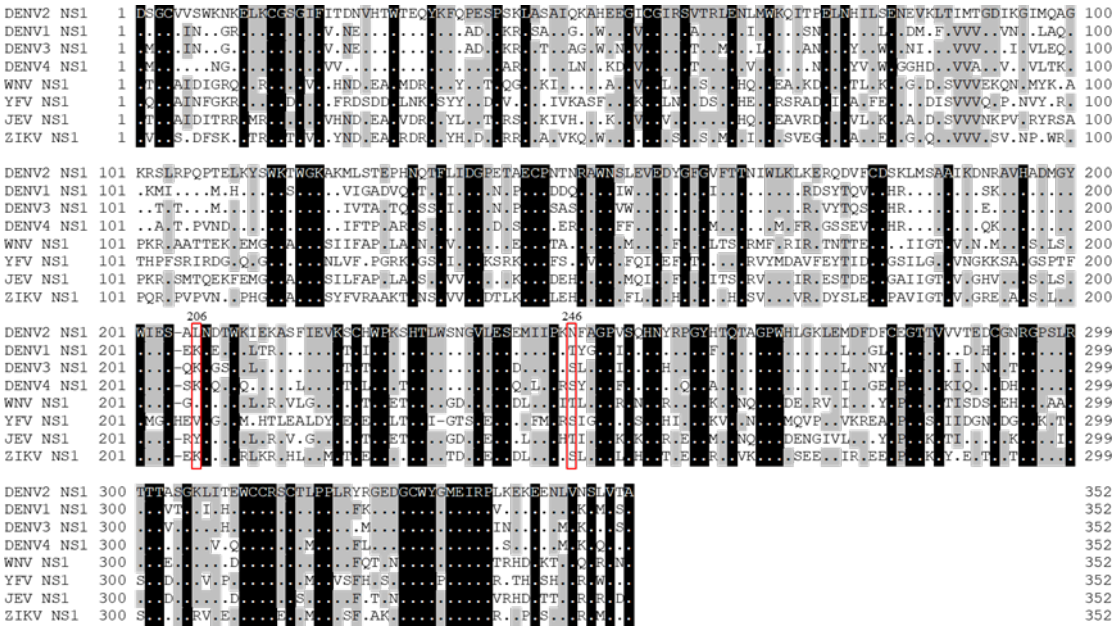

Figure 7. Amino acid sequences of flaviviruses NS5 MTase domain and NS1

(A) The black background indicates amino acids conserved in all flaviviruses, and the gray background shows amino acids shared in 50% or more of flaviviruses. The red rectangle indicates amino acid at position 130 of NS5. (B) The black background indicates amino acids conserved in all flaviviruses, and the gray background shows amino acids shared in 50% or more of flaviviruses. The red rectangles indicate amino acid at position 206 and 246 of NS1.

Summary

At the early stage of drug discovery, compound screening using a cultured cell infection system was performed to discover seeds of novel antiviral drug candidates against DENV and identify their mechanisms of action. MTT assay, which uses cell viability as an index, was performed as a screening method because DENV infection causes cell death in BHK-21 cells. First, using DENV2-infected BHK-21 cells, MTT assay was established and compound screening was performed using about 7,000 compounds retrieved from Shionogi & Co., Ltd. compound library.

As the result, three novel small molecules were identified which inhibit DENV replication. One novel compound with a benzimidazole skeleton, named Compound-B, was demonstrated antiviral activity specific to four DENV serotypes (EC_{50}: 1.32–4.12 μM). Analysis of a single amino acid substitution of Compound-B-resistant DENV2 revealed that mutation C87S in the NS4A contributes to resistance to Compound-B. Another two novel compounds with anti-DENV2 activity, tentatively named Compound-X and Compound-Y were identified as anti-DENV compound. Both compounds possess a quinolone skeleton, and the EC_{50}s of Compound-X and Compound-Y against DENV2 were 3.88 μM and 9.19 μM, respectively. Using mutational analysis, compounds-resistant DENV2 was obtained and a mutation V130A in the NS5 MTase domain was identified as cause of resistant to the quinolone compounds. However, these compounds did not inhibit MTase activity. In addition, incorporation of an additional NS1 N246D mutation with the NS5 V130A mutation in DENV2 resulted in recovery of viral replication and a further reduction of the sensitivity to the quinolone compounds by an unknown mechanism.

In this study, I discovered three novel anti-DENV compounds with novel mechanisms of action. The anti-DENV activity of these compounds is at micromolar level, therefore it is necessary to further improve the *in vitro* antiviral activity to show antiviral activity *in vivo*. These compounds target a previously unreported amino acid sites and are expected to lead to the development of novel antiviral drugs with novel mechanisms of action.

Chapter II: Efficacy of ensitrelvir against SARS-CoV-2 in a delayed-treatment mouse model

Introduction

COVID-19 is more likely to be severe in high-risk patients, including those with advanced age, cardiovascular disease, respiratory disease, renal disease, diabetes mellitus, obesity or immunodeficiency. Such patients present with rapidly progressive pneumonia, accompanied by symptoms including shortness of breath and dyspnea, and may require supplemental oxygen and even mechanical ventilation or extracorporeal membrane oxygenation. Severe COVID-19 disease is also characterized by thromboembolic disease and exhibits high mortality. The pandemic has led to severe pressure on and collapse of healthcare systems worldwide[49]. Development of vaccines against SARS-CoV-2 is an important strategy for preventing infection and transmission. However, the identification and development of antiviral agents to treat SARS-CoV-2 infections and prevent disease progression are also critical, especially in regard to breakthrough infections, unvaccinated individuals and situations in which the target pathogen is continually changing antigenically. Much of the initial effort aimed at identifying effective antivirals against COVID-19 has focused on identifying existing drugs for repurposing by screening their antiviral activity against SARS-CoV-2 *in vitro*. Unfortunately, this strategy has had limited success with frequent conflicting clinical outcomes[50].

Ensitrelvir (formerly named as S-217622) is a candidate compound that has been developed for the treatment of patients with COVID-19 and is an inhibitor of the SARS-CoV-2 3C-like (3CL) protease[51]. Ensitrelvir is created through structural optimization of seeds compound from SARS-CoV-2 3CL protease inhibitor in collaboration research between Hokkaido University and Shionogi & Co., Ltd. Ensitrelvir has strong antiviral activity *in vitro* and excellent pharmacokinetic profiles such as metabolic stability and oral absorption. The compound evaluation technology constructed in Chapter I is incorporated into the construction of an *in vitro* antiviral activity evaluation system for SARS-CoV-2 at Hokkaido University. Ensitrelvir has been shown to exhibit *in vitro* efficacy against various SARS-CoV-2 variants, including alpha, beta, gamma, delta, and omicron strains, and demonstrates *in vivo* efficacy in mice when administered immediately after SARS-CoV-2 infection[51]. The current study evaluated the inhibitory effect of ensitrelvir on SARS-CoV-2 replication in mice using a delayed-treatment model at the late stage of drug discovery. Mice infected with a gamma strain of SARS-CoV-2 were administered ensitrelvir or vehicle 24 hpi. Furthermore, using a mouse-adapted

SARS-CoV-2 strain that is highly pathogenic for mice[52], the effects of ensitrelvir was evaluated on symptoms such as lethality, weight loss, and inflammation in the lungs caused by viral infection. The findings should provide valuable insight into the *in vivo* efficacy of ensitrelvir in a model system using kinetics of intervention representative of real-world clinical settings.

Materials and methods

Ethics

The study complied with the Standards for the Reliability of Application Data (Article 43, Enforcement Regulations, Law for the Assurance of Quality, Efficacy, and Safety of Pharmaceuticals and Medical Devices). The animal protocols were approved by the Shionogi Pharmaceutical Research Center Institute Director (Shionogi & Co., Ltd., Toyonaka, Japan) based on the report of the Institutional Animal Care and Use Committee (Approval No. S21140D-0001 and S21068D-0008). The animal facilities were accredited by the Association for Assessment and Accreditation of Laboratory Animal Care (AAALAC) International.

Cell line and SARS-CoV-2 viruses

Transmembrane serine protease 2 (TMPRSS-2)-expressing VeroE6 (VeroE6/TMPRSS2) cells[53] were obtained from the Japanese Collection of Research Bioresources Cell Bank (Osaka, Japan) and maintained in DMEM (Thermo Fisher Scientific) containing 10% heat-inactivated FBS (Sigma-Aldrich) and 1% penicillin-streptomycin solution (Thermo Fisher Scientific). The SARS-CoV-2 gamma strain (hCoV-19/Japan/TY7-501/2021, Pango lineage P.1) was obtained from the National Institute of Infectious Diseases (NIID), Tokyo, Japan. The SARS-CoV-2 MA-P10 strain[52] (mouse-adapted hCoV-19/Japan/TY/WK-521/2020, Pango lineage A) was obtained from the Division of Molecular Pathobiology, International Institute for Zoonosis Control, Hokkaido University, Sapporo, Japan. The viruses were propagated in VeroE6/TMPRSS2 cells to prepare virus stocks, which were stored at −80°C. Viral titers were determined in VeroE6/TMPRSS2 cells using $TCID_{50}$ assays.

Animals

Female BALB/cAJcl mice were obtained from CLEA Japan, Inc. (Tokyo, Japan). All mice were maintained in a controlled environment of 20–26°C and 30–70% relative humidity with a 12 h light/dark cycle. Mice were housed 4–5 per cage with a standard chow diet of CE-2 (CLEA Japan, Inc.) and water was available ad libitum. Frozen virus stocks were diluted with Dulbecco's PBS (DPBS; Thermo Fisher Scientific) to prepare suspensions of 2.00×10^5 or 2.00×10^6 $TCID_{50}$/mL for the gamma strain and 6.00×10^4 $TCID_{50}$/mL for MA-P10. The mice were intranasally inoculated under anaesthesia at 5, 20, or 40 weeks of age with 50 μL of virus suspension per mouse. The animals were subsequently treated as described. Mice with >20% loss of initial body weight were

euthanized, according to humane endpoints.

Ensitrelvir preparation and dosing

The anti-SARS-CoV-2 test compound of ensitrelvir was used as an ensitrelvir fumaric acid co-crystal ($C_{22}H_{17}ClF_3N_9O_2 \cdot C_4H_4O_4$; Shionogi & Co. Ltd., Osaka, Japan) and freshly prepared in 0.5% (w/v) methylcellulose 400 cP (MC) solution (Fujifilm Wako Pure Chemical Corp., Osaka, Japan). According to a previous report[51], the ensitrelvir was orally administered twice daily, every 12 h, for 2, 3, or 5 days, as indicated, starting 24 hpi. The ensitrelvir was dosed at 0, 4, 8, 16, 32, or 64 mg (free-form mass)/kg of body weight, as indicated, in dosage volumes of 10 mL/kg of body weight.

Lung specimen/tissue collection and lung homogenate preparation

Mice (n = 3–5 per group) were euthanized 1, 2, 3, or 4 days post-infection (dpi) and their lungs removed. After homogenization of the lung samples with 2 mL of DPBS, the homogenates were centrifuged at 1,750 × *g* for 5 min at 4°C and filtered through a 0.45-μm filter. Homogenate aliquots were stored at −80°C until use.

Viral titer and RNA analysis

VeroE6/TMPRSS2 stocks were thawed and passaged several times in complete DMEM in 5% CO_2 at 37°C. Seventy-five microlitres of viral assay medium consisting of minimal essential medium (MEM) (Thermo Fisher Scientific) supplemented with 2% heat-inactivated FBS and 1% penicillin-streptomycin was added to the wells of 96-well plates. The cells were diluted to 1.5×10^5 cells/mL with viral assay medium and then seeded at 100 μL/well. Lung homogenates were serially diluted with viral assay medium. The diluted samples (25 μL) were added to the wells, and the plates were incubated in 5% CO_2 at 37°C for 4 days. After incubation, virus-induced CPE was evaluated under a microscope. Viral titers were expressed as $\log_{10}$ $TCID_{50}$/mL. If no CPE was observed at the lowest dilution, the titer was defined as 1.80 $\log_{10}$ $TCID_{50}$/mL. For RNA quantitation by RT-qPCR, lung homogenates (100 μL/sample) were placed in 96-well plates and inactivated with 300 μL of TRIzol LS (Thermo Fisher Scientific) for 1 min at room temperature. Total RNA was extracted from the inactivated samples using a Direct-zol-96 RNA Extraction Kit (Zymo Research, Irvine, CA, USA) according to the manufacturer's protocol. The samples were then analyzed using a MicroAmp Optical 384-Well Reaction Plate with Barcode (Thermo Fisher Scientific) and Applied Biosystems QuantStudio 5 Real-Time PCR System in conjunction with an EXPRESS One-Step SuperScript qRT-PCR Kit, universal (Thermo Fisher Scientific). The PCR

reaction mixes included 2 μL of extracted RNA, 0.4 μM Invitrogen forward primer 2019-nCoV_N1-F (5′-GAC CCC AAA ATC AGC GAA AT-3′; Thermo Fisher Scientific), 0.4 μM Invitrogen reverse primer 2019-nCoV_N1-R (5′-TCT GGT TAC TGC CAG TTG AAT CTG-3′; Thermo Fisher Scientific) and 0.25 μM probe 2019-nCoV_N1-P (5′-FAM-ACC CCG CAT TAC GTT TGG TGG ACC- TAMRA-3′; Eurofins, Tokyo, Japan) in total reaction volumes of 10 μL. The thermal cycling profile included one cycle of 50°C, 15 min; 95°C, 20 s followed by 40 cycles of 95°C, 3 s; 55°C, 30 s. Invitrogen synthetic single-stranded DNA (5′-ATA ATG GAC CCC AAA ATC AGC GAA ATG CAC CCC GCA TTA CGT TTG GTG GAC CCT CAG ATT CAA CTG GCA GTA ACC AGA ATG GAG-3′; Thermo Fisher Scientific) was 10-fold serially diluted and used to generate a standard curve. The samples were analyzed in duplicate.

Viral replication inhibition assay

Ensitrelvir and remdesivir (MedChemExpress, Monmouth Junction, NJ, USA) were weighed and dissolved in DMSO (Nacalai Tesque, Nakagyo-ku, Japan) to prepare 20 mmol/L solutions, which were then 3-fold serially diluted with DMSO. The diluted ensitrelvir and remdesivir solutions were subsequently diluted 100-fold with viral assay medium consisting of MEM supplemented with 2% FBS and 1% Penicillin-Streptomycin. One hundred microliters of the serially diluted ensitrelvir and remdesivir solutions were added to a 96-well plate. The SARS-CoV-2 MA-P10 strain virus stock solutions were diluted with viral assay medium to appropriate concentrations and dispensed at 50 μL/well into the 96-well plate containing test and reference substances. Then VeroE6/TMPRSS2 cells (50 μL), which were adjusted to 3.0×10^5 cells/mL, was dispensed into each well. The infectious dose of virus was 1.00×10^3 $TCID_{50}$/well with a multiplicity of infection of 0.067. The final concentrations of ensitrelvir were 0.0046, 0.014, 0.041, 0.12, 0.37, 1.1, 3.3, and 10 μmol/L. The final concentrations of remdesivir were 0.0091, 0.027, 0.082, 0.25, 0.74, 2.2, 6.7, and 20 μmol/L. The plate was mixed with a plate mixer and incubated at 37°C in a CO_2 incubator for 3 days. The assay was performed in duplicate for each substance concentration.

The inhibitory effects of the test and reference substances on CPE induced by SARS-CoV-2 were measured based on cell viability as previously repoted[51]. Briefly, after three days of incubation, 60 μL of CellTiter-Glo 2.0 Assay Reagent (Promega Corporation) was added to each well. After mixing, the cells were incubated at room temperature for approximately 30 min, and 200 μL of each sample was dispensed into a new white 96-well plate. The luminescent signal (Relative Light Unit [RLU]) was measured using an EnSpire multiplate reader (PerkinElmer) with the following

parameters: mode of measurement by rows = bi-directional, measurement height = 0.2 mm, and measurement time = 0.1 second/well. The % inhibition of CPE induced by SARS-CoV-2 was calculated using the following formula:

$$\% \text{ inhibition} = (X - Z1)/(Y - Z1) \times 100$$

Where X = RLU of the test substance well; Y = the average RLU of cell control wells; and Z1 = the average RLU of virus control wells. The cell-control wells were without virus infection and not treated with any test or reference substance; the virus-control wells were infected with virus but not treated with test or reference substance. The concentrations achieving EC_{50} were calculated using software XLfit 5.3.1.3 (fit model: 205). Finally, the mean and SD values were calculated for three independent experiments.

Evaluation of body weight, lung weight, lung histopathology, and nucleocapsid immunohistochemistry

Mouse survival and body weights were monitored and recorded at the indicated timepoints. Specifically, 20-week-old mice (n = 5) infected with the SARS-CoV-2 gamma strain and 40-week-old mice (n = 4–8) infected with MA-P10 were examined for survival and weighed daily from Day 0 through to Day 14. Whole-lung weight of 40-week-old mice infected with MA-P10 (n = 5–10) was measured 4 dpi. For histopathological analysis, left lungs of 40-week-old mice infected with MA-P10 (n = 3–5) were fixed in 10% neutral buffered formalin 4 dpi, paraffin-embedded, sectioned at 3 μm thickness, and stained with haematoxylin and eosin (H&E). Pathological evaluation was performed by modifying the Owen's report[54]. Blinded histopathological evaluations for alveolar epithelial degeneration or necrosis, bronchial or bronchiolar epithelial degeneration or necrosis, vascular endothelial degeneration or necrosis, alveolar/interstitial inflammation, bronchial or bronchiolar inflammation, perivascular inflammation, and thrombosis were independently performed by two pathologists. The lung pathology parameters were scored 0 (normal), 1 (minimal), 2 (mild), 3 (moderate), and 4 (marked). Total histopathological scores for individual mice were calculated by adding the individual histopathological scores, and mean total histopathological scores were calculated for each group. Disparate scores between the pathologists were resolved by the first pathologist rescoring the specimen.

Immunohistochemical (IHC) staining of the left lungs of 40-week-old mice infected with MA-P10 was also performed 4 dpi. Briefly, deparaffinized sections were treated with citric acid buffer (pH 6.0) for 10 min at 121°C using an autoclave for antigen retrieval. The sections were incubated with 3% hydrogen peroxide followed by blocking with normal goat serum. The sections were incubated overnight at 4°C with a primary

rabbit polyclonal antibody against the SARS-CoV-2 nucleocapsid protein (1:1,000; Cat. No. ab281297; Abcam, Cambridge, UK). The sections were then incubated for 30 min at room temperature with a horseradish peroxidase-labelled secondary polyclonal antibody (Cat. No. 414341; Nichirei Biosciences Inc., Tokyo, Japan). The target antigen was detected using 3,3′-diaminobenzidine as a chromogen. The sections were counterstained with haematoxylin and evaluated under a microscope. Semi-quantitative grading of the IHC staining was performed using the following outcomes: −, no staining detected; ±, minimal staining; +, mild staining; ++, moderate staining; +++, marked staining.

Cytokine/chemokine analysis

Cytokine/chemokine levels of tumor necrosis factor-α (TNF-α), interleukin (IL)-1β, IL-6, IFN-γ, and monocyte chemoattractant protein-1 (MCP-1) were measured in lung homogenates of 40-week-old mice that were non-infected (n = 2) or infected with MA-P10 and treated twice daily for 3 days with vehicle (MC; n = 3) or ensitrelvir (8 or 32 mg/kg body weight; n = 5) starting 24 hpi. The lungs were then harvested and homogenates processed 4 dpi. Mouse TNF-α Immunoassay (MTA00B), Mouse IL-1β Immunoassay (MLB00C), Mouse IL-6 Immunoassay (M6000B), Mouse INF-γ Immunoassay (MIF00), and Mouse/Rat CCL2/JE/MCP-1 Immunoassay (MJE00B) Quantikine enzyme-linked immunosorbent assay (Enzyme-linked immunosorbent assay [ELISA]) kits were purchased from R&D Systems (Minneapolis, MN, USA). The assays were performed according to the manufacturer's instructions. The plates were read using an EnSpire microplate reader (PerkinElmer) at 450 nm, using 570 nm for correction. The results were quantitated using 4-parameter logistic curve-fit against 2-fold serially diluted standards of each cytokine/chemokine.

Statistical analysis

Statistical analysis was performed using SAS Version 9.4 software (SAS Institute, Cary, NC, USA). The two-sided significance level was set at $P = 0.05$. Mean body weight uniformity among the different experimental groups was confirmed by one-way analysis of variance (ANOVA). Endpoint analysis of lung viral titers was measured using a logarithmic scale. To assess ensitrelvir effects on viral titers, the RNA and cytokine/chemokine levels in the lungs of each ensitrelvir-treated group were compared with that of the vehicle-treated group at each timepoint. Dunnett's method was applied to adjust for multiplicity of multiple testing. Survival time comparisons between each ensitrelvir-treated group and the vehicle-treated group were analyzed by log-rank test. Proportion comparisons of current body weight to initial body weight between the

experimental groups at each timepoint were analyzed using one-way ANOVA with equal variance assumption, including the fixed effect of group and contrast method by the analyzed timepoints. For mice that died during the experimental period, the proportion of current body weight to initial body weight was imputed at 80% for all timepoints post-death. The fixed-sequence procedure was used to adjust the multiplicity of statistical tests for survival time and body weight analyses.

Results

Effect of ensitrelvir on viral titers and RNA levels in lungs of 5-week-old BALB/cAJcl mice infected with the SARS-CoV-2 gamma strain

To initially evaluate the *in vivo* effect of ensitrelvir on SARS-CoV-2, 5-week-old mice were infected with 1.00×10^4 $TCID_{50}$ of the SARS-CoV-2 gamma strain and then orally administered various doses of ensitrelvir or vehicle twice daily starting 24 hpi. While all the mice survived, the subsequent analysis revealed that ensitrelvir had a dose-dependent antiviral effect on the viral titers of the SARS-CoV-2 gamma strain in the lungs of infected mice (Figure 8A). Both 32 and 64 mg/kg ensitrelvir treatments resulted in significant reduction of viral titers 2 and 3 dpi as compared with that of vehicle treatments ($P < 0.0001$). In addition, 8 and 16 mg/kg ensitrelvir treatments significantly reduced lung viral titers at 3 dpi ($P < 0.05$ and $P < 0.01$, respectively). Likewise, ensitrelvir dose-dependently reduced viral RNA levels of the SARS-CoV-2 gamma strain (Figure 8B). Compared with the vehicle-treated group, treatment with ensitrelvir significantly reduced the amount of viral RNA in the lungs of infected mice 2 and 3 dpi at doses of 16 mg/kg ($P < 0.01$ and $P < 0.05$, respectively), 32 mg/kg ($P < 0.01$ and $P < 0.0001$, respectively) and 64 mg/kg ($P < 0.0001$ and $P < 0.0001$, respectively). A significant reduction was also observed with 8 mg/kg ensitrelvir treatment as compared with the vehicle-treated group at 3 dpi ($P < 0.05$). When 5-week-old BALB/cAJcl mice were infected with 1.00×10^5 $TCID_{50}$ of the SARS-CoV-2 gamma strain, their body weight declined to approximately 90% of their original mass on 3 or 4 dpi, which was quickly recovered (data not shown).

Effect of ensitrelvir on body weight of 20-week-old BALB/cAJcl mice infected with the SARS-CoV-2 gamma strain

Host factors, including age, are key determinants of disease severity and progression for COVID-19, both in humans[55] and mice[56, 57]. Therefore, I evaluated the effect of ensitrelvir in older (20-week-old) mice infected with SARS-CoV-2. As an indicator of disease progression, the mice were monitored for body weight loss caused by infection with 1.00×10^5 $TCID_{50}$ of the SARS-CoV-2 gamma strain (Figure 9). Body weight loss was observed in vehicle-treated mice infected with the SARS-CoV-2 gamma strain starting at 3 dpi; however, the weight loss was significantly suppressed from 3 to 8 dpi with administration of ≥8 mg/kg ensitrelvir ($P < 0.05$). Furthermore, the body weight of ensitrelvir-treated mice was not significantly different from that of non-infected control mice. No mortality was observed in any of the experimental groups.

A B

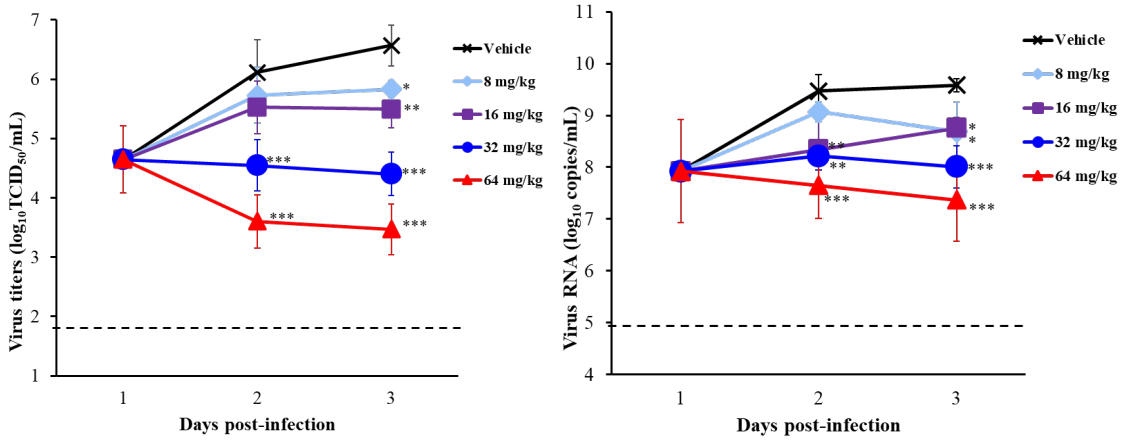

Figure 8. Effect of ensitrelvir on viral titers and RNA levels in 5-week-old female BALB/cAJcl mice infected with SARS-CoV-2 gamma strain (hCoV-19/Japan/TY7-501/2021)

The mice were nasally infected with 1.00×10^4 $TCID_{50}$ of the SARS-CoV-2 gamma strain and then orally administered various doses of ensitrelvir or vehicle (0.5% MC solution) every 12 h (twice daily) for two days. The first administration was performed 24 hpi. (A) Viral titers in lungs of mice were determined using VeroE6/TMPRSS2 cells. Each point represents the mean ± SD of five mice. The dashed line represents the lower limit of quantification (LLOQ, 1.80 $\log_{10}$ $TCID_{50}$/mL). *P*-values were calculated by Dunnett's method versus vehicle. **P* < 0.05, ***P* < 0.01, ****P* < 0.0001. (B) Viral RNA levels in the lungs of mice were determined using RT-qPCR. Each point represents the mean ± SD of five mice. The dashed line represents the LLOQ (4.92 $\log_{10}$ copies/mL). *P*-values were calculated by Dunnett's method versus vehicle. **P* < 0.05, ***P* < 0.01, ****P* < 0.0001.

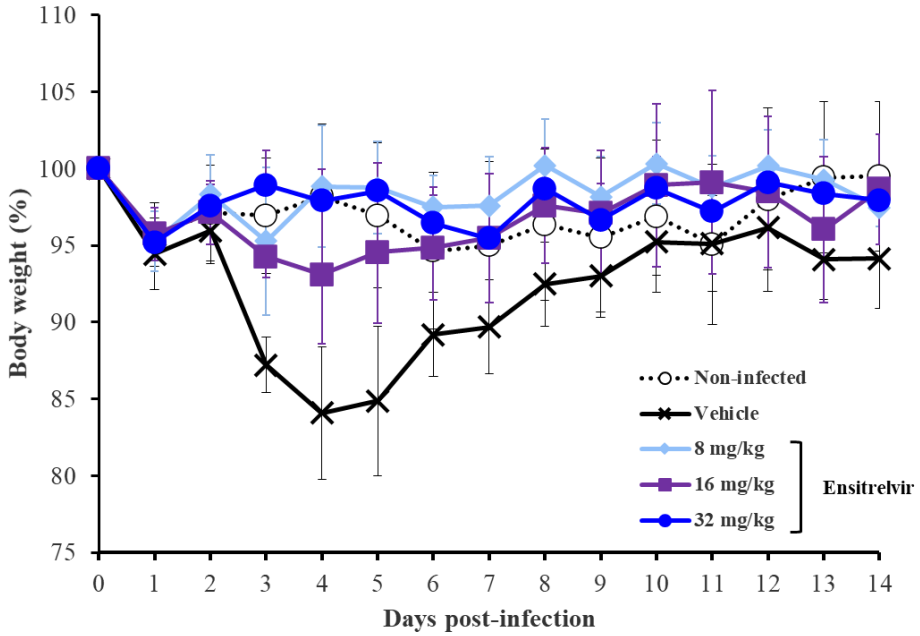

Figure 9. Effect of ensitrelvir on the body weight of 20-week-old female BALB/cAJcl mice infected with SARS-CoV-2 gamma strain (hCoV-19/Japan/TY7-501/2021)

The mice were nasally infected with 1.00×10^5 $TCID_{50}$ of the SARS-CoV-2 gamma strain and then orally administered various doses of ensitrelvir or vehicle (0.5% MC solution) every 12 h (twice daily) for five days. The first administration was performed 24 hpi. Results are presented as the percentage of current body weight as compared with that of initial body weight prior to infection. Each point represents the mean ± SD of five mice.

Effect of ensitrelvir on 40-week-old BALB/cAJcl mice infected with SARS-CoV-2 MA-P10

To further increase the severity of SARS-CoV-2 infection in the test system, aged (retired; 40-week-old) mice were infected with 3.00×10^3 $TCID_{50}$ of the mouse-adapted SARS-CoV-2 MA-P10 strain[52]. Infected mice were orally administered various doses of ensitrelvir or vehicle twice daily for 5 days starting 24 hpi. The mice were then monitored for survival and body weight loss. The results showed that ensitrelvir improved the survival rates of mice in a dose-dependent manner (Figure 10A). While improved survival was not observed with 4 mg/kg ensitrelvir as compared with that of vehicle-treated mice, survival time significantly improved for infected mice treated with 8 mg/kg ($P < 0.05$), 16 mg/kg ($P < 0.001$), and 32 mg/kg ($P < 0.001$) ensitrelvir. Ensitrelvir treatment also suppressed the body weight loss observed in mice treated with vehicle and did so in a dose-dependent manner (Figure 10B). Significant protection from body weight loss compared with that of the vehicle-treated group was observed 2 dpi with 32 mg/kg ensitrelvir ($P < 0.01$), 3 dpi with 16 mg/kg ($P < 0.01$) and 32 mg/kg ($P < 0.001$) ensitrelvir, and 4 and 5 dpi with 8 mg/kg ($P < 0.01$), 16 mg/kg ($P < 0.001$), and 32 mg/kg ($P < 0.001$) ensitrelvir.

Ensitrelvir also effectively reduced MA-P10 titers in the lungs of infected 40-week-old mice (Figure 11A). Ensitrelvir treatment at 8 mg/kg significantly reduced lung viral titers compared with that of vehicle treatment at 4 dpi ($P < 0.05$), while treatment with 32 mg/kg ensitrelvir reduced viral levels at 2 dpi ($P < 0.01$), 3 dpi ($P < 0.0001$), and 4 dpi ($P < 0.0001$). This *in vivo* activity was consistent with the *in vitro* effect of ensitrelvir inhibiting CPE in MA-P10-infected VeroE6/TMPRSS2 cells. Briefly, the mean EC_{50} of ensitrelvir against MA-P10 ± SD, based on three independent experiments, was 0.12 ± 0.04 μmol/L compared with that of 1.6 ± 0.1 μmol/L for remdesivir.

Treatment of SARS-CoV-2 MA-P10-infected 40-week-old mice 24 hpi with ensitrelvir also resulted in dose-dependent suppression of inflammatory cytokine/chemokine production 4 dpi, including TNF-α, IL-1β, IL-6, and MCP-1 (Figure 11B). Ensitrelvir at a dose of 32 mg/kg restored the levels of all the cytokines examined to those at or near levels observed in non-infected mice. In a previous study, the lung weight of mice increased following influenza virus infection, along with increased infiltration of inflammatory cells[58]. Therefore, the lung weight of SARS-CoV-2 MA-P10-infected mice were analyzed in the current study, and found it had increased compared with that of non-infected mice. However, treatment with 32 mg/kg ensitrelvir significantly suppressed the lung weight increases 4 dpi as compared with that of vehicle-treated mice (Figure 11C). Furthermore, at 4 dpi, TNF-α, IL-6, and MCP-1 levels

positively correlated with the viral titers, and IL-1β, IL-6, and MCP-1 levels positively correlated with the lung weights (Figure 12).

Consistent with the cytokine/chemokine and lung weight results, lung histopathology revealed degeneration and necrosis of alveolar, bronchial, or bronchiolar epithelium cells and vascular endothelial cells, as well as the presence of inflammation and thrombus, in vehicle-treated mice infected with SARS-CoV-2 MA-P10 (Figure 11D). In contrast, the severity of these infection- related pulmonary lesions was reduced in mice treated with 32 mg/kg ensitrelvir starting 24 hpi. Furthermore, the amount of positive immunostaining for virus nucleocapsid was reduced in MA-P10-infected mice treated with 32 mg/kg ensitrelvir as compared with that of vehicle-treated mice.

A

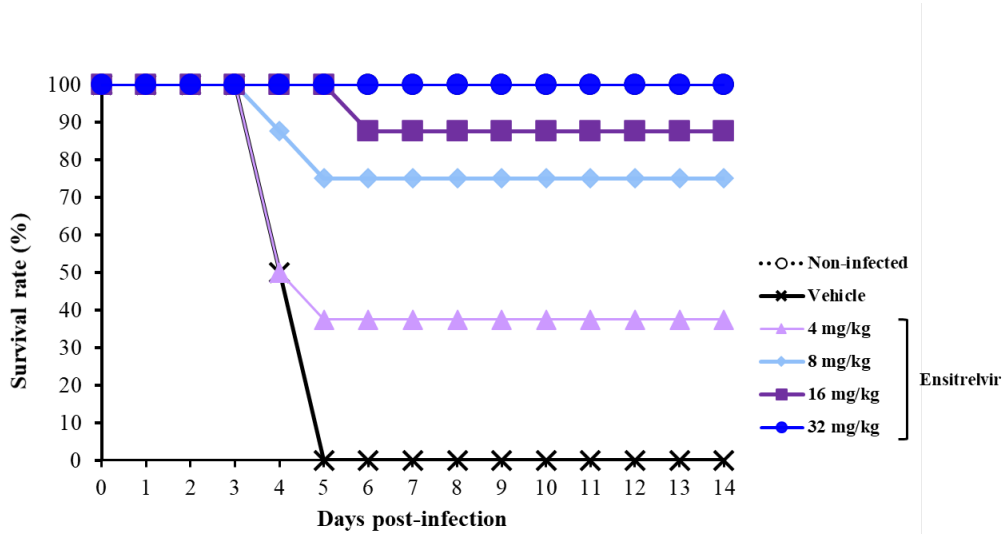

B

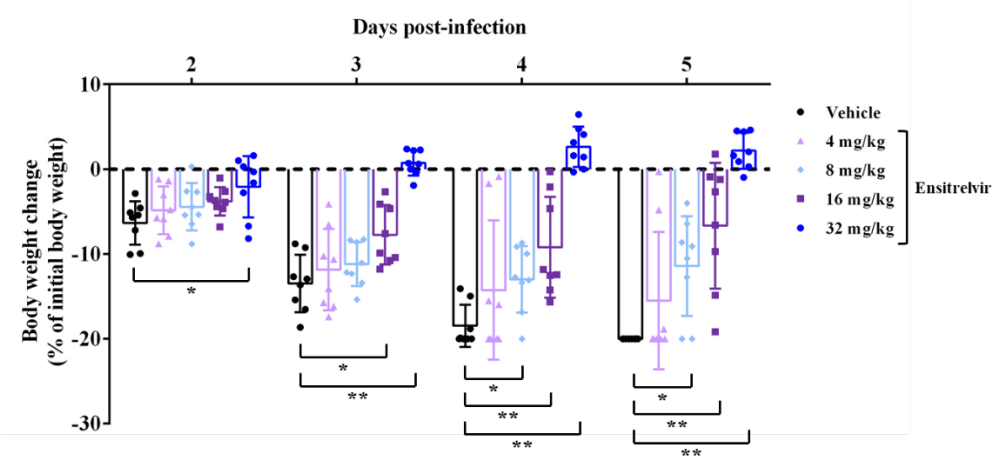

Figure 10. Effect of ensitrelvir on survival and the body weight of 40-week-old female BALB/cAJcl mice infected with mouse-adapted SARS-CoV-2 MA-P10

The mice were nasally infected with 3.00×10^3 $TCID_{50}$ of the SARS-CoV-2 MA-P10 and then orally administered various doses of ensitrelvir or vehicle (0.5% MC solution) every 12 h (twice daily) for five days. The first administration was performed 24 hpi. (A) Mouse survival was monitored daily, and survival curves generated using Kaplan-Meier analysis. n = 4 mice/group for non-infected mice and n = 8 mice/group for infected mice. *P*-values were calculated using log-rank test versus vehicle (multiplicity was adjusted by fixed-sequence procedure). $*P < 0.05$ and $**P < 0.001$. (B) Body-weight values are presented as a percentage of initial body weight for 2–5 dpi. The graph bars represent the mean ± SD of 4 mice/group for non-infected mice and 8

mice/group for infected mice. *P*-values were calculated using ANOVA-test versus vehicle (multiplicity was adjusted by fixed-sequence procedure). *$P < 0.01$ and **$P < 0.001$.

A

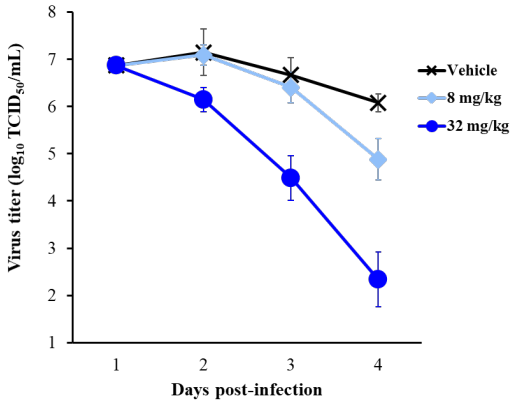
Virus titer (log_{10} $TCID_{50}$/mL)
Days post-infection
Vehicle
8 mg/kg
32 mg/kg

B

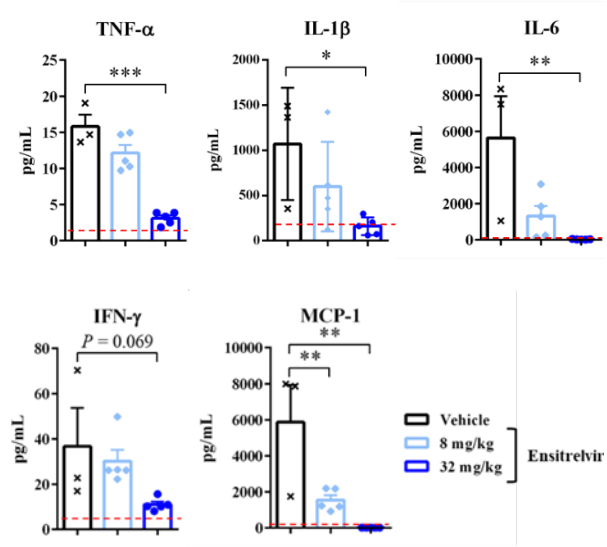
TNF-α
IL-1β
IL-6
IFN-γ
MCP-1
pg/mL
P = 0.069
Vehicle
8 mg/kg
32 mg/kg
Ensitrelvir

C

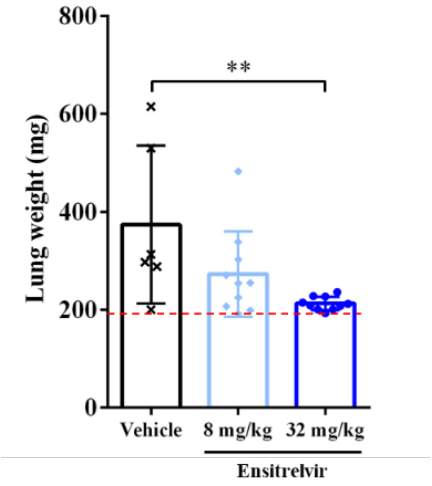
Lung weight (mg)
Vehicle
8 mg/kg
32 mg/kg
Ensitrelvir

D

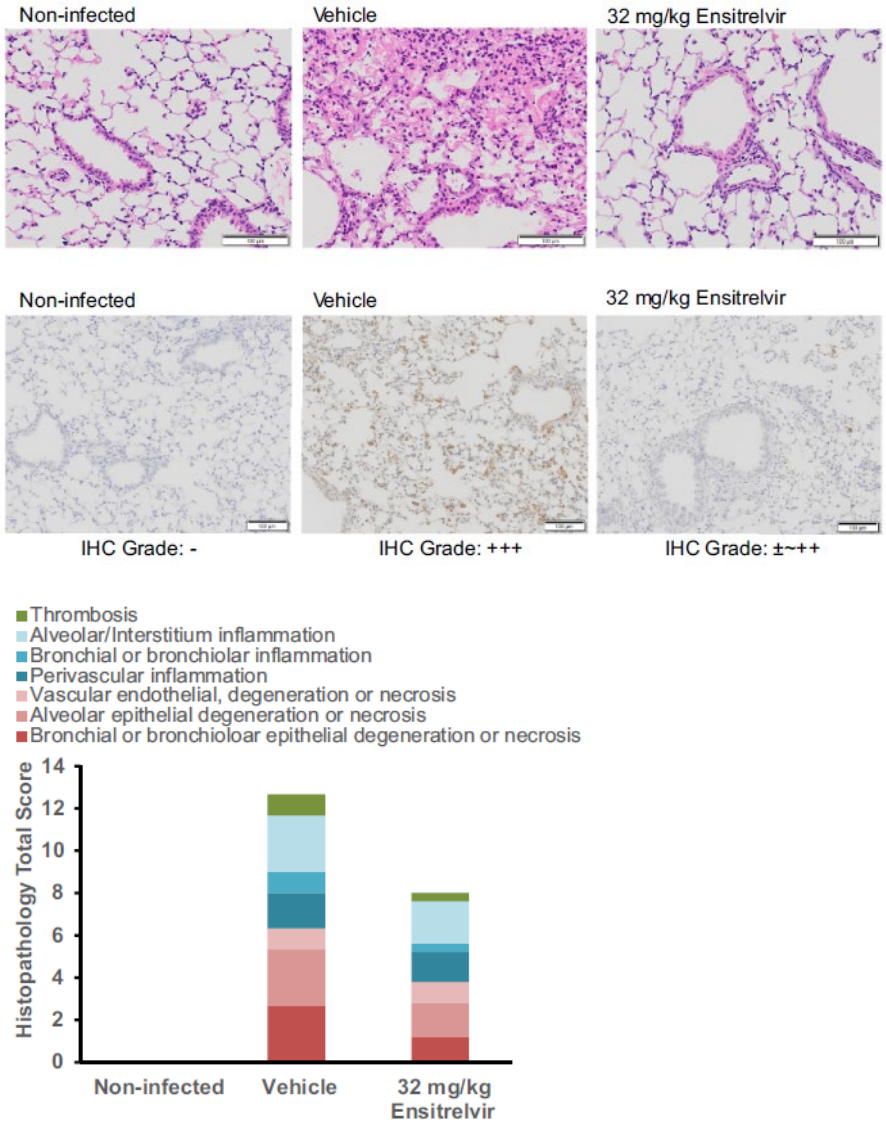

Figure 11. Effect of ensitrelvir on viral titer, cytokine/chemokine production, lung weight, and lung pathology in 40-week-old female BALB/cAJcl mice infected with mouse-adapted SARS-CoV-2 MA-P10

The mice were infected with 3.00×10^3 $TCID_{50}$ of the SARS-CoV-2 MA-P10 and then orally administered various doses of ensitrelvir or vehicle (0.5% MC solution) every 12 h (twice daily) for three days. The first administration was performed 24 hpi. (A) Viral titers in the lungs were determined using VeroE6/TMPRSS2 cells. Each point represents the mean ± SD. The dashed line represents LLOQ of 1.80 $\log_{10}$ $TCID_{50}$/mL. *P*-values were calculated by Dunnett's method versus vehicle. $^*P < 0.05$, $^{**}P < 0.01$, $^{***}P < 0.0001$. n = 5 mice/group except day 4 of the vehicle-treated group for which n = 3. (B)

Cytokine/chemokine levels in mouse lungs 4 dpi were determined using ELISA assays. The red lines indicate cytokine/chemokine levels detected in non-infected control mice (n = 2). The graph bars represent the mean ± SD. *P*-values were calculated by Dunnett's multiple comparison test versus vehicle. **P* < 0.05, ***P* < 0.01, ****P* < 0.001. n = 5 mice/group except the vehicle-treated group for which n = 3. (C) Lung weight of vehicle-treated (n = 6) and ensitrelvir-treated (8 mg/kg and 32 mg/kg) (n = 10) mice 4 dpi. The red lines indicate lung weight of non-infected control mice (n = 3). The graph bars represent the mean ± SD. *P*-values were calculated by Dunnett's method versus vehicle. ***P* < 0.01. (D) Histopathology of the lung assessed by H&E staining (upper panels) and IHC staining of viral nucleocapsid (lower panels). Mice treated with 32 mg/kg ensitrelvir (n = 3) exhibited less lung pathology and reduced IHC staining for virus capsid as compared with that of the vehicle-treated group (n = 5). Non-infected control mice (n = 3) were negative for IHC staining. IHC Grade: −, Not detected; ±, Minimal; +, Mild; ++, Moderate; +++, Marked. Data from dead mice were excluded from the analysis.

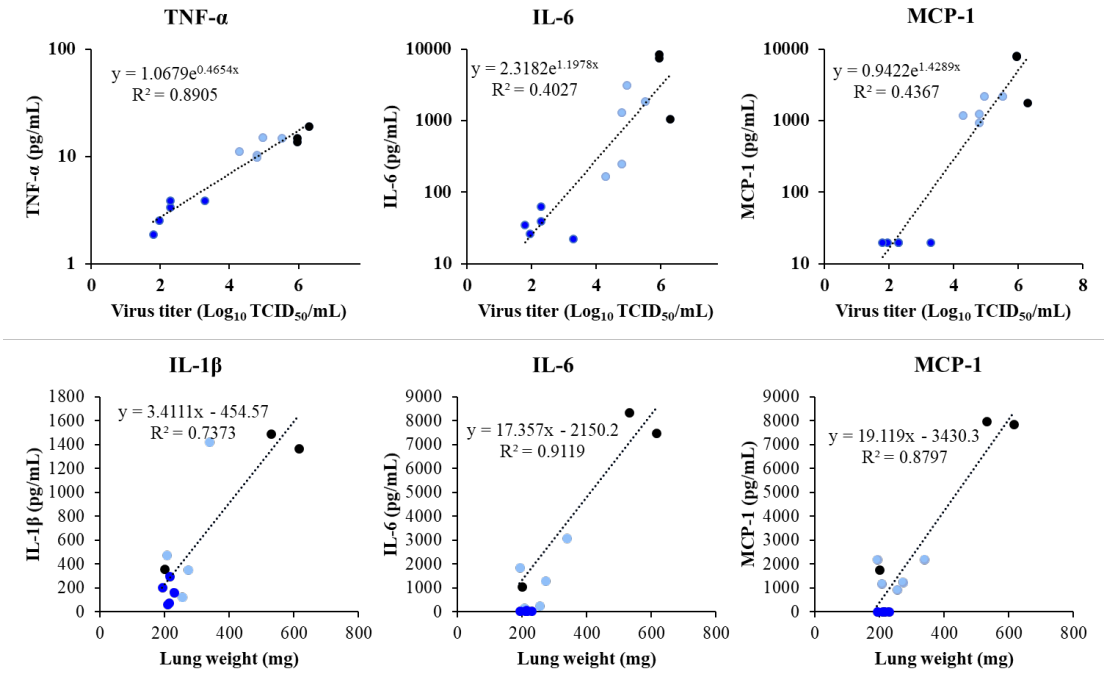

Figure 12. Correlation of virus titer and lung weight with cytokine/chemokine levels
Each dot represents an individual animal. Vehicle (black dots), 8 mg/kg ensitrelvir (light blue dots), and 32 mg/kg ensitrelvir (dark blue dots).

Discussion

The current study demonstrated that ensitrelvir reduced SARS-CoV-2 virus levels in a dose-dependent manner compared with that of vehicle treatments, as indicated by infectious viral titers and viral RNA levels in the lungs of infected mice. Furthermore, the antiviral activity correlated with increased survival, reduced body weight loss, reduced pulmonary lesions and suppression of inflammatory cytokine/chemokine levels. Importantly, the observed *in vivo* effects of ensitrelvir occurred in a delayed-treatment model system. Ensitrelvir shows high selectivity against the 3CL protease[51] and the body weight changes of infected mice were similar to that of non-infected mice administered 32 mg/kg ensitrelvir. Accordingly, no ensitrelvir-associated toxicity was observed in the mice of this study.

Ensitrelvir is an inhibitor of the SARS-CoV-2 3CL protease, which is essential for processing of the SARS-CoV-2-encoded polyprotein, as well as viral replication[59]. The 3CL proteases of SARS-CoV-2 and other coronaviruses, such as feline infectious peritonitis virus and porcine deltacoronavirus, are known to antagonize innate immune function, including the inhibition of type I IFN signaling and participation in the transforming growth factor-β (TGF-β) signaling pathway[60-62]. Furthermore, the 3CL protease-mediated cleavage of NLR family pyrin domain containing 12 (NLRP12) may explain the hyperinflammatory response observed in patients with severe COVID-19[63, 64]. Elevated IL-6 levels have also been correlated with increased mortality in patients with COVID-19[65]. Thus, the findings in the current study of ensitrelvir repressing IL-6 expression may suggest its potential for reducing mortality in patients with COVID-19. The 3CL protease is an ideal antiviral target for SARS-CoV-2, its variants and potential future viruses as it is conserved among coronaviruses. Moreover, it plays a critical role in viral replication, yet there are no known human host-cell proteases with the same substrate specificity[59].

According to a previous report, patients with COVID-19 have significantly elevated levels of inflammatory markers, such as IL-1β and IFNγ[66]. In addition, the concentration of MCP-1 and TNF-α in patients with severe illness are higher than those in patients with mild COVID-19[66], suggesting that cytokine storms contribute to disease severity. Moreover, elevated levels of these inflammatory markers were also observed in mouse lungs using my infection model, but their expression was suppressed by ensitrelvir treatment. The positive correlation between inflammatory markers and viral titers suggests that ensitrelvir, through its antiviral effect, is able to suppress the production of components of the cytokine storm caused by SARS-CoV-2 infection, thus imparting a

protective effect on lung structure.

Small-animal models that recapitulate SARS-CoV-2 infection and disease are critical for studying COVID-19 and for evaluating potential vaccines and therapeutics. The use of mice and mouse-adapted virus strains as model systems has been previously documented[56, 57]. My current findings also demonstrate the utility of the model for SARS-CoV-2 replication, infection, and pathogenesis studies, thus making it a powerful resource for evaluating the efficacy of antivirals against SARS-CoV-2 and in preventing COVID-19 progression. Nirmatrelvir, another 3CL protease inhibitor, shows antiviral activity in a mice model when treatment is started 4 hpi[54]. In the current study, ensitrelvir also showed antiviral activity in a delayed-treatment mouse model. This suggests that 3CL protease inhibitors are effective against SARS-CoV-2 in mice, even after the initiation of infection. These two compounds will be directly compared in future studies.

The current study did have certain limitations. For instance, differences do exist between humans and mice. Importantly, ensitrelvir exhibits lower clearance and longer half-lives in non-rodents compared with that in rodents[51]. Accordingly, I performed twice-daily administration of ensitrelvir to the mice, while once-daily administration in clinical treatment. Furthermore, while evaluation of ensitrelvir included both a SARS-CoV-2 gamma and a mouse-adapted strain, no direct evidence was provided regarding its efficacy against other SARS-CoV-2 variants. However, conservation of 3CL proteases and their importance in the virus life cycle suggest that the *in vivo* efficacy of ensitrelvir is likely against a broad range of SARS-CoV-2 strains, as well as potentially against other coronaviruses. This hypothesis remains to be comprehensively investigated.

Summary

SARS-CoV-2 is the etiological agent of COVID-19 and a devastating worldwide health concern. Development of safe and effective treatments is not only important for interventions during the current pandemic, but also for providing general treatment options moving forward. Ensitrelvir have been developed as an antiviral compound that targets the 3CL protease of SARS-CoV-2.

In this study, a delayed-treatment mouse model was used to clarify the potential *in vivo* efficacy of ensitrelvir at the late stage of drug discovery. Female BALB/cAJcl mice of different ages were infected with the SARS-CoV-2 gamma strain (hCoV-19/Japan/TY7-501/2021) or mouse-adapted SARS-CoV-2 MA-P10 and then 24 hpi orally administered various doses of ensitrelvir or vehicle. Based on infectious viral titers and viral RNA levels in the lungs of infected mice, ensitrelvir reduced viral loads in a dose-dependent manner. The antiviral efficacy correlated with increased survival, reduced body weight loss, reduced pulmonary lesions, and suppression of inflammatory cytokine/chemokine levels.

This study is the first evaluation of the *in vivo* anti-SARS-CoV-2 efficacy of ensitrelvir in a delayed-treatment mouse model. In this model, ensitrelvir demonstrated high antiviral potential and suppressed lung inflammation and lethality caused by SARS-CoV-2 infection. The findings support the continued clinical development of ensitrelvir as an antiviral agent to treat patients with COVID-19.

Conclusion

This study provided a new insight that will contribute to the discovery of novel antiviral drug candidates through the research of early drug discovery against DENV and late drug discovery against SARS-CoV-2.

In Chapter I, at the early stage of drug discovery, cell-based assay using DENV2 infected BHK-21 cells was constructed and screened 7,000 compounds for finding seeds of antiviral drug candidate. Compound-B, classified as an HCV RdRp inhibitor, possesses a benzimidazole skeleton with antiviral activity against DENV1, 2, 3, and 4 at the micromolar level. Two novel compounds having quinolone skeleton, termed Compound-X and Compound-Y, had anti-DENV2 activity at micromolar levels. Furthermore, their targets were identified through the isolation of resistant viruses and analysis using infectious clones with amino acid substitutions. It is presumed that the target of Compound-B is NS4A C87 and that of Compound-X and Compound-Y is NS5 MTase domain V130. The target amino acid sites of these compounds have not been previously reported, therefore it is expected to create antiviral drugs with novel mechanisms of action. It is expected that the information of this research will lead to the development of novel antiviral drugs by improving the antiviral activity and the kinetics to create a compound that exhibits *in vivo* efficacy. In the future, I will optimize the structure of the seeds of antiviral drug candidate, create an *in vivo* infection model using the knowledge and technology obtained from the mouse infection model conducted in Chapter II, and select antiviral drug candidates that shows *in vivo* efficacy.

In Chapter II, *in vivo* evaluation against SARS-CoV-2 was performed at the late stage of drug discovery, demonstrated therapeutic efficacy in delayed *in vivo* administration of the COVID-19 therapeutic candidate compound ensitrelvir. In a mouse infection model using SARS-CoV-2 gamma strain, I first evaluated the effect of ensitrelvir on reducing viral titer in lung and suppression of body weight. Furthermore, using mouse-adapted MA-P10 strain that show high pathogenicity to mice, the suppression of lethality, lung disease, and cytokine/chemokine production by the ensitrelvir treatment were observed, in addition to the effect of reducing virus titer in lung and suppression of body weight loss, showed potential to improve clinical symptoms. These results demonstrated its potential as an antiviral agent to treat COVID-19 patients and support continued clinical development. Furthermore, ensitrelvir received emergency approval as a therapeutic drug for the novel SARS-CoV-2 infection in Japan on November 22, 2022, and demonstrated clinical efficacy. The results of this study are expected to have contributed significantly to the development of a therapeutic drug for COVID-19.

In the future, I will confirm effect of ensitrelvir about prevention of infection and suppression of transmission *in vivo*, which will lead to verification of the efficacy of ensitrelvir in preventing and suppressing transmission of COVID-19 in clinical settings.

Treatment methods for various viral infections, not only DENV and SARS-CoV-2, are limited, and the results of this research are expected to contribute to the development of new antiviral drugs for other virus infection.

Acknowledgments

I would like to acknowledge Professor Hirofumi Sawa and Associate Professor Yasuko Oba, Division of molecular Pathobiology, International institute for Zoonosis Control, Hokkaido University, for valuable advice, suggestions, and encouragement throughout the study.

I would also great appreciation to Professor Yoshihiro Sakoda, Laboratory of Microbiology, Department of Disease Control, Division of Veterinary Medicine, Faculty of Veterinary Medicine, Hokkaido University, for his valuable advice and detained review of this manuscript.

I am also deeply grateful to Guest Professor Akihiko Sato and Mr. Kei Konishi, Division of Anti-Virus Drug Research, Shionogi & Co. Ltd., International institute for Zoonosis Control, Hokkaido University, for intellectual discussion, critical review, and suggestions throughout the study.

I thank Dr. Tomohiko Takasaki (BML, Inc., Tokyo, Japan) and Dr. Shigeru Tajima (NIID, Tokyo, Japan) for their kind offer of experimental materials and technical supports.

I acknowledge the NIID for providing the SARS-CoV-2 gamma strain (hCoV-19/Japan/TY7-501/2021). I also acknowledge Prof. Hirofumi Sawa (Hokkaido University, Sapporo, Japan) for providing the SARS-CoV-2 MA-P10 strain. I am grateful to all my colleagues who participated in the COVID-19 antiviral program at Shionogi & Co., Ltd. and thank Shionogi Techno-Advance Research Co., Ltd. for technical support in the pharmacological studies.

References

1. Bhatt S, Gething PW, Brady OJ, Messina JP, Farlow AW, Moyes CL, Drake JM, Brownstein JS, Hoen AG, Sankoh O, Myers MF, George DB, Jaenisch T, Wint GR, Simmons CP, Scott TW, Farrar JJ, Hay SI. The global distribution and burden of dengue. *Nature*, 496 (7446), 504-507, 2013.
2. Messina JP, Brady OJ, Scott TW, Zou C, Pigott DM, Duda KA, Bhatt S, Katzelnick L, Howes RE, Battle KE, Simmons CP, Hay SI. Global spread of dengue virus types: mapping the 70 year history. *Trends Microbiol*, 22 (3), 138-146, 2014.
3. World Health Organization. Weekly epidemiological update on COVID-19 - 21 December 2022. Edition 123. https://www.who.int/publications/m/item/covid-19-weekly-epidemiological-update---21-december-2022.
4. J Woolhouse ME, Adair K, Brierley L. RNA Viruses: A Case Study of the Biology of Emerging Infectious Diseases. *Microbiol Spectr*, 1 (1), 1-11, 2013
5. Poltronieri P, Sun B, Mallardo M. RNA Viruses: RNA Roles in Pathogenesis, Coreplication and Viral Load. *Curr Genomics*, 16 (5), 327-335, 2015.
6. Guzman MG, Halstead SB, Artsob H, Buchy P, Farrar J, Gubler DJ, Hunsperger E, Kroeger A, Margolis HS, Martínez E, Nathan MB, Pelegrino JL, Simmons C, Yoksan S, Peeling RW. Dengue: a continuing global threat. *Nat Rev Microbiol*, 8 (12 Suppl), S7-S16, 2010.
7. Rigau-Pérez JG, Clark GG, Gubler DJ, Reiter P, Sanders EJ, Vorndam AV. Dengue and dengue haemorrhagic fever. *Lancet*, 352 (9132), 971-977, 1998.
8. World Health Organization, 2017. Dengue and severe dengue [WWW Document]. http://www.who.int/mediacentre/factsheets/fs117/en/ (accessed 2.5.18).
9. Kraemer MU, Sinka ME, Duda KA, Mylne AQ, Shearer FM, Barker CM, Moore CG, Carvalho RG, Coelho GE, Van Bortel W, Hendrickx G, Schaffner F, Elyazar IR, Teng HJ, Brady OJ, Messina JP, Pigott DM, Scott TW, Smith DL, Wint GR, Golding N, Hay SI. The global distribution of the arbovirus vectors *Aedes aegypti* and *Ae. Albopictus*. *eLlife*, 4, e08347, 2015.
10. Sirisena PD, Noordeen F. Evolution of dengue in Sri Lanka-changes in the virus, vector, and climate. *Int J Infect Dis*, 19, 6-12, 2014.
11. Aguiar M, Stollenwerk N, Halstead SB. The Impact of the Newly Licensed Dengue Vaccine in Endemic Countries. *PLoS Negl Trop Dis*, 10 (12), e0005179, 2016.
12. Capeding MR, Tran NH, Hadinegoro SR, Ismail HI, Chotpitayasunondh T, Chua MN, Luong CQ, Rusmil K, Wirawan DN, Nallusamy R, Pitisuttithum P, Thisyakorn U, Yoon IK, van der Vliet D, Langevin E, Laot T, Hutagalung Y, Frago C, Boaz M,

Wartel TA, Tornieporth NG, Saville M, Bouckenooghe A; CYD14 Study Group. Clinical efficacy and safety of a novel tetravalent dengue vaccine in healthy children in Asia: a phase 3, randomised, observer-masked, placebo-controlled trial. *Lancet*, 384 (9951), 1358-1365, 2014.

13. Sabchareon A, Wallace D, Sirivichayakul C, Limkittikul K, Chanthavanich P, Suvannadabba S, Jiwariyavej V, Dulyachai W, Pengsaa K, Wartel TA, Moureau A, Saville M, Bouckenooghe A, Viviani S, Tornieporth NG, Lang J. Protective efficacy of the recombinant, live-attenuated, CYD tetravalent dengue vaccine in Thai schoolchildren: a randomised, controlled phase 2b trial. *Lancet*, 380 (9853), 1559-1567, 2012.
14. Rivera L, Biswal S, Sáez-Llorens X, Reynales H, López-Medina E, Borja-Tabora C, Bravo L, Sirivichayakul C, Kosalaraksa P, Martinez Vargas L, Yu D, Watanaveeradej V, Espinoza F, Dietze R, Fernando L, Wickramasinghe P, Duarte MoreiraJr E, Fernando AD, Gunasekera D, Luz K, Venâncioda Cunha R, Rauscher M, Zent O, Liu M, Hoffman E, LeFevre I, Tricou V, Wallace D, Alera M, Borkowski A. Three-year Efficacy and Safety of Takeda's Dengue Vaccine Candidate (TAK-003). *Clin Infect Dis*, 75 (1), 107-117, 2022.
15. Nascimento EJM, Norwood B, Kpamegan E, Parker A, Fernandes J, Perez-Guzman E, Tricou V, Braun R, Sharma M, Dean HJ. Antibodies Produced in Response to a Live-Attenuated Dengue Vaccine are Functional in Activating the Complement System. *J Infect Dis*, 2022. Online ahead of print.
16. Lim SP, Wang QY, Noble CG, Chen YL, Dong H, Zou B, Yokokawa F, Nilar S, Smith P, Beer D, Lescar J, Shi PY. Ten years of dengue drug discovery: progress and prospects. *Antiviral Res*, 100 (2), 500-519, 2013
17. Kuno G, Chang GJ, Tsuchiya KR, Karabatsos N, Cropp CB. Phylogeny of the genus Flavivirus. *J Virol*, 72 (1), 73-83, 1998.
18. Henchal EA, Putnak JR. The Dengue Viruses. *Clin Microbiol Rev*, 3 (4), 376-396, 1990.
19. Holmes EC, Twiddy SS. The origin, emergence and evolutionary genetics of dengue virus. *Infect Genet Evol*, 3 (1), 19-28, 2003.
20. Kuhn RJ, Zhang W, Rossmann MG, Pletnev SV, Corver J, Lenches E, Jones CT, Mukhopadhyay S, Chipman PR, Strauss EG, Baker TS, Strauss JH. Structure of dengue virus: Implications for flavivirus organization, maturation, and fusion. *Cell*, 108 (5), 717-725, 2002.
21. Dong H, Fink K, Züst R, Lim SP, Qin CF, Shi PY. Flavivirus RNA methylation. *J Gen Virol*, 95 (Pt 4), 763-778, 2014.

22. Lim SP, Noble CG, Shi PY. The dengue virus NS5 protein as a target for drug discovery. *Antiviral Res*, 119, 57-67, 2015.
23. Ackermann M, Padmanabhan R. De Novo Synthesis of RNA by the Dengue Virus RNA-dependent RNA Polymerase Exhibits Temperature Dependence at the Initiation but Not Elongation Phase. *J Biol Chem*, 276 (43), 39926-39937, 2001.
24. Koonin EV. The phylogeny of RNA-dependent RNA polymerases of positive-strand RNA viruses. *J Gen Virol*, 72 (Pt 9), 2197-2206, 1991.
25. Pauwels R, Balzarini J, Baba M, Snoeck R, Schols D, Herdewijn P, Desmyter J, De Clercq E. Rapid and automated tetrazolium-based colorimetric assay for the detection of anti-HIV compounds. *J Virol Methods*, 20 (4), 309-321, 1988.
26. Sasaki M, Orba Y, Ueno K, Ishii A, Moonga L, Hang'ombe BM, Mweene AS, Ito K, Sawa H. Metagenomic analysis of the shrew enteric virome reveals novel viruses related to human stool-associated viruses. *J Gen. Virol*, 96 (Pt 2), 440-452, 2015.
27. Yozwiak NL, Skewes-Cox P, Gordon A, Saborio S, Kuan G, Balmaseda A, Ganem D, Harris E, DeRisi JL. Human enterovirus 109: a novel interspecies recombinant enterovirus isolated from a case of acute pediatric respiratory illness in Nicaragua. *J Virol*, 84 (18), 9047-9058, 2010.
28. Tajima S, Nukui Y, Ito M, Takasaki T, Kurane I. Nineteen nucleotides in the variable region of 3' non-translated region are dispensable for the replication of dengue type 1 virus *in vitro*. *Virus Res*, 116 (1-2), 38-44, 2006.
29. Kato F, Kobayashi T, Tajima S, Takasaki T, Miura T, Igarashi T, Hishiki T. Development of a novel Dengue-1 virus replicon system expressing secretory Gaussia luciferase for analysis of viral replication and discovery of antiviral drugs. *Jpn J Infect Dis*, 67 (3), 209-212, 2014.
30. Boonyasuppayakorn S, Padmanabhan R. Construction of plasmid, bacterial expression, purification, and assay of dengue virus type 2 NS5 methyltransferase. *Methods Mol Biol*, 1138, 361-373, 2014.
31. Chung KY, Dong H, Chao AT, Shi PY, Lescar J, Lim SP. Higher catalytic efficiency of N-7-methylation is responsible for processive N-7 and 2′-O methyltransferase activity in dengue virus. *Virology*, 402 (1), 52-60, 2010.
32. Diamond MS, Zachariah M, Harris E. Mycophenolic acid inhibits dengue virus infection by preventing replication of viral RNA. *Virology*, 304 (2), 211-221, 2002.
33. Ishida T, Suzuki T, Hirashima S, Mizutani K, Yoshida A, Ando I, Ikeda S, Adachi T, Hashimoto H. Benzimidazole inhibitors of hepatitis C virus NS5B polymerase: identification of 2-[(4-diarylmethoxy)phenyl]-benzimidazole. *Bioorg Med Chem Lett*, 16 (7), 1859-1863, 2006.

34. Karam P, Powdrill MH, Liu HW, Vasquez C, Mah W, Bernatchez J, Götte M, Cosa G. Dynamics of hepatitis C virus (HCV) RNA-dependent RNA polymerase NS5B in complex with RNA. *J Biol Chem*, 289 (20), 14399-14411, 2014.
35. Tomei L, Altamura S, Bartholomew L, Biroccio A, Ceccacci A, Pacini L, Narjes F, Gennari N, Bisbocci M, Incitti I, Orsatti L, Harper S, Stansfield I, Rowley M, De Francesco R, Migliaccio G. Mechanism of action and antiviral activity of benzimidazole-based allosteric inhibitors of the hepatitis C virus RNA-dependent RNA polymerase. *J Virol*, 77 (24), 13225-13231, 2003.
36. Tarantino D, Cannalire R, Mastrangelo E, Croci R, Querat G, Barreca ML, Bolognesi M, Manfroni G, Cecchetti V, Milani M. Targeting flavivirus RNA dependent RNA polymerase through a pyridobenzothiazole inhibitor. *Antiviral Res*, 134, 226-235, 2016.
37. Miller S, Kastner S, Krijnse-Locker J, Bühler S, Bartenschlager R. The non-structural protein 4A of dengue virus is an integral membrane protein inducing membrane alterations in a 2K-regulated manner. *J Biol Chem*, 282 (12), 8873-8882, 2007.
38. Hung YF, Schwarten M, Hoffmann S, Willbold D, Sklan EH, Koenig B. Amino Terminal Region of Dengue Virus NS4A Cytosolic Domain Binds to Highly Curved Liposomes. *Viruses*, 7 (7), 4119-4130, 2015.
39. Teo CS, Chu JJ. Cellular vimentin regulates construction of dengue virus replication complexes through interaction with NS4A protein. *J Virol*, 88 (4), 1897-1913, 2014.
40. Lee CM, Xie X, Zou J, Li SH, Lee MY, Dong H, Qin CF, Kang C, Shi PY. Determinants of Dengue Virus NS4A Protein Oligomerization. *J Virol*, 89 (12), 6171-6183, 2015.
41. Zou J, Xie X, Wang QY, Dong H, Lee MY, Kang C, Yuan Z, Shi PY. Characterization of Dengue Virus NS4A and NS4B Protein Interaction. *J Virol*, 89 (7), 3455-3470, 2015.
42. He Z, Zhu X, Wen W, Yuan J, Hu Y, Chen J, An S, Dong X, Lin C, Yu J, Wu J, Yang Y, Cai J, Li J, Li M. Dengue Virus Subverts Host Innate Immunity by Targeting Adaptor Protein MAVS. *J Virol*, 90 (16), 7219-7230, 2016.
43. Soto-Acosta R, Bautista-Carbajal P, Cervantes-Salazar M, Angel-Ambrocio AH, Del Angel RM. DENV up-regulates the HMG-CoA reductase activity through the impairment of AMPK phosphorylation: A potential antiviral target. *PLoS Pathog*, 13 (4), e1006257, 2017.
44. Zhou Y, Ray D, Zhao Y, Dong H, Ren S, Li Z, Guo Y, Bernard KA, Shi PY, Li H. Structure and function of flavivirus NS5 methyltransferase. *J Virol*, 81 (8), 3891-3903, 2007.

45. Winkler G, Maxwell SE, Ruemmler C, Stollar V. Newly synthesized dengue-2 virus nonstructural protein NS1 is a soluble protein but becomes partially hydrophobic and membrane-associated after dimerization. *Virology*, 171 (1), 302-305, 1989.
46. Lindenbach BD and Rice CM. Genetic Interaction of Flavivirus Nonstructural Proteins NS1 and NS4A as a Determinant of Replicase Function. *J Virol*, 73 (6), 4611-4621, 1999.
47. Youn S, Li T, McCune BT, Edeling MA, Fremont DH, Cristea IM, Diamond MS. Evidence for a Genetic and Physical Interaction between Nonstructural Proteins NS1 and NS4B That Modulates Replication of West Nile Virus. *J Virol*, 86 (13), 7360-7371, 2012.
48. Flamand M, Megret F, Mathieu M, Lepault J, Rey FA, Deubel V. Dengue Virus Type 1 Nonstructural Glycoprotein NS1 Is Secreted from Mammalian Cells as a Soluble Hexamer in a Glycosylation-Dependent Fashion. *J Virol*, 73 (7), 6104-6110, 1999.
49. Helmy YA, Fawzy M, Elaswad A, Sobieh A, Kenney SP, Shehata AA. The COVID-19 pandemic: a comprehensive review of taxonomy, genetics, epidemiology, diagnosis, treatment, and control. *J Clin Med*, 9 (4), 1225, 2020.
50. Izda V, Jeffries MA, Sawalha AH. COVID-19: a review of therapeutic strategies and vaccine candidates. *Clin Immunol*, 222, 108364, 2021.
51. Unoh Y, Uehara S, Nakahara K, Nobori H, Yamatsu Y, Yamamoto S, Maruyama Y, Taoda Y, Kasamatsu K, Suto T, Kouki K, Nakahashi A, Kawashima S, Sanaki T, Toba S, Uemura K, Mizutare T, Ando S, Sasaki M, Orba Y, Sawa H, Sato A, Sato T, Kato T, Tachibana Y. Discovery of S-217622, a non-covalent oral SARS-CoV-2 3CL protease inhibitor clinical candidate for treating COVID-19. *J Med Chem*, 65 (9), 6499-6512, 2022.
52. Uemura K, Nobori H, Sato A, Toba S, Kusakabe S, Sasaki M, Tabata K, Matsuno K, Maeda N, Ito S, Tanaka M, Anraku Y, Kita S, Ishii M, Kanamitsu K, Orba Y, Matsuura Y, Hall WW, Sawa H, Kida H, Matsuda A, Maenaka K. *BioRxiv*, doi: https://doi.org/10.1101/2022.12.14.520006
53. Matsuyama S, Nao N, Shirato K, Kawase M, Saito S, Takayama I, Nagata N, Sekizuka T, Katoh H, Kato F, Sakata M, Tahara M, Kutsuna S, Ohmagari N, Kuroda M, Suzuki T, Kageyama T, Takeda M. Enhanced isolation of SARS-CoV-2 by TMPRSS2-expressing cells. *Proc Nat Acad Sci USA*, 117 (13), 7001-7003, 2020.
54. Owen DR, Allerton CMN, Anderson AS, Aschenbrenner L, Avery M, Berritt S, Boras B, Cardin RD, Carlo A, Coffman KJ, Dantonio A, Di L, Eng H, Ferre R, Gajiwala KS, Gibson SA, Greasley SE, Hurst BL, Kadar EP, Kalgutkar AS, Lee JC, Lee J, Liu W, Mason SW, Noell S, Novak JJ, Obach RS, Ogilvie K, Patel NC, Pettersson M,

Rai DK, Reese MR, Sammons MF, Sathish JG, Singh RSP, Steppan CM, Stewart AE, Tuttle JB, Updyke L, Verhoest PR, Wei L, Yang Q, Zhu Y. An oral SARS-CoV-2 Mpro inhibitor clinical candidate for the treatment of COVID-19. *Science*, 374 (6576), 1586-1593, 2021.

55. Chen Y, Klein SL, Garibaldi BT, Li H, Wu C, Osevala NM, Li T, Margolick JB, Pawelec G, Leng SX. Aging in COVID-19: vulnerability, immunity and intervention. *Aging Res Rev*, 65, 101205, 2021.
56. Gu H, Chen Q, Yang G, He L, Fan H, Deng YQ, Wang Y, Teng Y, Zhao Z, Cui Y, Li Y, Li XF, Li J, Zhang NN, Yang X, Chen S, Guo Y, Zhao G, Wang X, Luo DY, Wang H, Yang X, Li Y, Han G, He Y, Zhou X, Geng S, Sheng X, Jiang S, Sun S, Qin CF, Zhou Y. Adaptation of SARS-CoV-2 in BALB/c mice for testing vaccine efficacy. *Science*, 369 (6511), 1603-1607, 2020.
57. Sun S, Gu H, Cao L, Chen Q, Ye Q, Yang G, Li RT, Fan H, Deng YQ, Song X, Qi Y, Li M, Lan J, Feng R, Guo Y, Zhu N, Qin S, Wang L, Zhang YF, Zhou C, Zhao L, Chen Y, Shen M, Cui Y, Yang X, Wang X, Tan W, Wang H, Wang X, Qin CF. Characterization and structural basis of a lethal mouse-adapted SARS-CoV-2. *Nat Comm*, 12 (1), 5654, 2021.
58. Fukao K, Noshi T, Yamamoto A, Kitano M, Ando Y, Noda T, Baba K, Matsumoto K, Higuchi N, Ikeda M, Shishido T, Naito A. Combination treatment with the cap-dependent endonuclease inhibitor baloxavir marboxil and a neuraminidase inhibitor in a mouse model of influenza A virus infection. *J Antimicrob Chemother*, 74 (3), 654-662, 2019.
59. Ullrich S, Nitsche C. The SARS-CoV-2 main protease as drug target. *Bioorg Med Chem Lett*, 30 (17), 127377, 2020.
60. Moustaqil M, Ollivier E, Chiu HP, Van Tol S, Rudolffi-Soto P, Stevens C, Bhumkar A, Hunter DJB, Freiberg AN, Jacques D, Lee B, Sierecki E, Gambin Y. SARS-CoV-2 proteases PLpro and 3CLpro cleave IRF3 and critical modulators of inflammatory pathways (NLRP12 and TAB1): implications for disease presentation across species. *Emerg Microbes Infect*, 10 (1), 178-195, 2021.
61. Chen S, Tian J, Li Z, Kang H, Zhang J, Huang J, Yin H, Hu X, Qu L. Feline infectious peritonitis virus Nsp5 inhibits type I interferon production by cleaving NEMO at multiple sites. *Viruses*, 12 (1), 43, 2019.
62. Zhu X, Chen J, Tian L, Zhou Y, Xu S, Long S, Wang D, Fang L, Xiao S. Porcine deltacoronavirus nsp5 cleaves DCP1A to decrease its antiviral activity. *J Virol*, 94 (15), e02162-19, 2020.
63. Chen G, Wu D, Guo W, Cao Y, Huang D, Wang H, Wang T, Zhang X, Chen H, Yu H,

Zhang X, Zhang M, Wu S, Song J, Chen T, Han M, Li S, Luo X, Zhao J, Ning Q. Clinical and immunological features of severe and moderate coronavirus disease 2019. *J Clin Invest*, 130 (5), 2620-2629, 2020.

64. Giamarellos-Bourboulis EJ, Netea MG, Rovina N, Akinosoglou K, Antoniadou A, Antonakos N, Damoraki G, Gkavogianni T, Adami ME, Katsaounou P, Ntaganou M, Kyriakopoulou M, Dimopoulos G, Koutsodimitropoulos I, Velissaris D, Koufargyris P, Karageorgos A, Katrini K, Lekakis V, Lupse M, Kotsaki A, Renieris G, Theodoulou D, Panou V, Koukaki E, Koulouris N, Gogos C, Koutsoukou A. Complex immune dysregulation in COVID-19 patients with severe respiratory failure. *Cell Host Microbe*, 27 (6), 992-1000, 2020.
65. Zhou F, Yu T, Du R, Fan G, Liu Y, Liu Z, Xiang J, Wang Y, Song B, Gu X, Guan L, Wei Y, Li H, Wu X, Xu J, Tu S, Zhang Y, Chen H, Cao B. Clinical course and risk factors for mortality of adult inpatients with COVID-19 in Wuhan, China: a retrospective cohort study. *Lancet*, 395 (10229), 1054-1062, 2020.
66. Huang C, Wang Y, Li X, Ren L, Zhao J, Hu Y, Zhang L, Fan G, Xu J, Gu X, Cheng Z, Yu T, Xia J, Wei Y, Wu W, Xie X, Yin W, Li H, Liu M, Xiao Y, Gao H, Guo L, Xie J, Wang G, Jiang R, Gao Z, Jin Q, Wang J, Cao B. Clinical features of patients infected with 2019 novel coronavirus in Wuhan, China. *Lancet*, 395 (10223), 497-506, 2020.

Summary in Japanese (和文要旨)

これまで様々なウイルス感染症が世界中で発生、流行している。感染や重症化を抑制するためのワクチン開発も実施されているが、感染症のコントロールには治療薬の開発も必須である。デングウイルス (DENV) は熱帯及び亜熱帯地域における最も深刻な感染症の 1 つであるデング熱及びデング出血熱の原因ウイルスであるが、DENV 感染症に対する抗ウイルス薬は存在していない。また、重症急性呼吸器症候群コロナウイルス 2 (SARS-CoV-2) は、新型コロナウイルス感染症 (COVID-19) の病原体であり、2019 年 11 月に中国で確認されて以降、世界的な流行が国際社会の公衆衛生において非常に深刻な問題となっている。抗 SARS-CoV-2 作用を有する治療薬は存在しているものの、薬効が不十分あるいは安全性、薬物相互作用などに懸念があり、新規抗ウイルス薬の開発が望まれている。

抗ウイルス薬は多くのプロセスを経て開発される。創薬初期段階では、*in vitro* において、ウイルスが保有する酵素活性やウイルス感染細胞におけるウイルス増殖などを指標としたアッセイ法などを用いて、化合物スクリーニングを行い、抗ウイルス薬候補のシーズを得ることが必要である。このシーズは、化合物の官能基等を変換して構造を最適化し、*in vitro* における薬効を高めるとともに、代謝安定性、経口吸収性などの薬物動態も考慮して抗ウイルス薬候補となる。創薬後期段階では、*in vitro* における薬効のみならず、マウス感染モデル等の *in vivo* における薬効を示す化合物の中から、臨床で治療効果を示す可能性を有する抗ウイルス薬候補が選択される。

本研究は DENV 及び SARS-CoV-2 を対象として、新規抗ウイルス薬の開発に寄与する知見を獲得することを目的として、第 I 章では DENV を対象とした創薬初期段階である抗ウイルス薬候補のシーズの探索を実施した。また、第 II 章では SARS-CoV-2 を対象として、COVID-19 治療薬候補のエンシトレルビルについて、創薬後期段階であるマウス感染モデルを用いた *in vivo* での薬効評価を実施した。

第 I 章では、培養細胞感染系を用いた化合物スクリーニングにより新規抗 DENV 化合物を選抜し、更にその作用メカニズムを明らかにした。化合物スクリーニング方法として、DENV 2 型 (DENV2) の接種により細胞死を引き起こすハムスター由来の BHK-21 細胞に約 7,000 個の化合物を作用させて、各化合物による細胞死の抑制を判定する方法を用いた。その結果、抗 DENV2 活性を持つ新規化合物として、ベンズイミダゾール骨格を有する化合物 B 及び、キノロン骨格を有する化合物 X 並びに化合物 Y を見出した。化合物 B、化合物 X、化合物 Y は DENV2 に対して薬剤の有効性の指標である 50%効果濃度（EC_{50}）が 1.32、

3.88、9.19 μM の抗ウイルス活性を示した。次に、本化合物の標的部位を同定することを目的として、化合物存在下で DENV2 を継代し、化合物耐性ウイルス分離を試みたところ、ウイルスゲノムに数ヶ所のアミノ酸変異が確認された。認められた変異と化合物の作用の関係を確認するために、リバースジェネティクス法を用いて、アミノ酸置換ウイルスを作製し、化合物に対する感受性の変化を評価した結果、DENV2 の膜タンパク質である非構造タンパク質 4A (NS4A) の C87S の変異が化合物 B に対する感受性低下に寄与することが明らかになった。また化合物 X 並びに化合物 Y は、NS5 のメチルトランスフェラーゼドメインの V130A の変異が当該化合物に対する感受性低下に寄与することを明らかにした。

第 II 章では、北海道大学と塩野義製薬の共同研究において、SARS-CoV-2 の 3C 様プロテアーゼを標的とした化合物スクリーニングから得られた化合物の構造を最適化することにより得られたエンシトレルビルを対象として、SARS-CoV-2 の *in vivo* 感染モデルを用いて薬効を評価した。本化合物は、第 I 章で記載した化合物評価技術の活用により抗ウイルス活性が見出され、これまでにオミクロン株を含む様々な SARS-CoV-2 変異株に対して *in vitro* での有効性が示されている。また、代謝安定性、経口吸収性などの薬物動態プロファイルが優れており、マウス感染モデルにおいて感染直後に投与することにより、用量依存的な抗ウイルス効果が認められていた。しかし、臨床現場では、抗ウイルス薬投与は感染直後ではなく、感染から一定時間後に投与が開始される。そこで本研究では、SARS-CoV-2 の経鼻接種から一定時間後にエンシトレルビル投与を開始した際の *in vivo* での薬効を評価した。具体的には SARS-CoV-2 ガンマ株をマウスに経鼻接種後 24 時間でエンシトレルビル投与を開始し、肺内ウイルス量の減少及び体重減少抑制効果を評価した。更に、マウスに対して高病原性を示す SARS-CoV-2 マウス馴化株 (MA-P10) を用いて、エンシトレルビル投与により、MA-P10 株感染によって生じる、致死、体重減少、肺の炎症等の所見に対する影響を評価した。その結果、エンシトレルビルは感染マウスの肺内ウイルス力価、ウイルス RNA 量共に、用量依存的に減少させ、本効果が、生存率の改善、体重減少の抑制、肺病変の減少、及び炎症性サイトカイン/ケモカインの産生抑制と相関していることを明らかにした。

以上より、第 I 章では DENV2 感染細胞の細胞生存率を指標とした化合物スクリーニングにより抗 DENV 活性を有する新規化合物及びその標的部位を同定し、複数の新規メカニズムを有する抗ウイルス薬候補のシーズを見出した。今回見出された抗 DENV 活性を有する新規化合物の抗ウイルス活性は μM レベルであり、更なる抗ウイルス活性の向上が必要と考えられるが、今後、当該候補化合物の構造を最適化し、第 II 章で実施したマウス感染モデルで得られた知識・技術を活用して *in vivo* 感染モデルを構築し、*in vivo* での薬効を示す抗ウイルス薬候

補を選抜することが期待される。

第 II 章では COVID-19 治療薬候補として開発されたエンシトレルビルを対象として、SARS-CoV-2 感染 24 時間後からの投与における *in vivo* での抗ウイルス活性及び症状改善効果を確認した。本研究で得られた結果により、エンシトレルビルが臨床においても抗ウイルス活性を示し、かつ COVID-19 症状を改善する治療効果を発揮することが期待され、COVID-19 治療薬として臨床開発のステージに進むことが可能になった。更にエンシトレルビルは 2022 年 11 月 22 日、日本において COVID-19 に係る治療薬として緊急承認を得られており、本研究成果は COVID-19 治療薬の創製に大きく貢献したと思われる。今後、非臨床の *in vivo* 感染モデルで感染予防効果、伝播抑制効果等の効果を確認することにより、臨床現場における COVID-19 の予防、伝播抑制効果に対するエンシトレルビルの有効性の検証に繋げることを目指す。

本研究で示した抗ウイルス薬候補のシーズ探索手法や *in vivo* における薬効評価方法を他のウイルスに応用することで、様々なウイルスに対する抗ウイルス薬の開発も期待される。